RICE UNIVERSITY

In-vivo Studies of C_{60}-Bis(bisphosphonate) and Synthesis of a C_{60}-Bisphosphonate-Beta-Blocker Conjugate for the Prevention and Treatment of Osteoporosis

by

Ivana Romina Guadalupe Peralta

A THESIS SUBMITTED
IN PARTIAL FULFILLMENT OF THE
REQUIREMENTS FOR THE DEGREE

Doctor of Philosophy

APPROVED, THESIS COMMITTEE:

Lon J. Wilson, Professor of Chemistry, Chair

Catherine G. Ambrose, Associate Professor and
Director of Research

Robert H. Hauge, Distinguished Faculty Fellow
in Chemistry

HOUSTON, TEXAS

DECEMBER 2009

ProQuest LLC
789 East Eisenhower Parkway
P.O. Box 1346
Ann Arbor, MI 48106-1346

ABSTRACT

In-vivo Studies of C_{60}-Bis(bisphosphonate) and Synthesis of a C_{60}-Bisphosphonate-Beta-Blocker Conjugate for the Prevention and Treatment of Osteoporosis

by

Ivana Romina Guadalupe Peralta

Fullerene (C_{60}) derivatives have been extensively studied for a variety of medical applications, which include neuroprotective agents, HIV-1 protease inhibitors, photodynamic cancer therapeutics, medical contrast agents and radiotracers, slow release systems for aerosol liposome delivery, immunotherapy agents, and transfection vectors. The first part of this work is dedicated to the study of the *in-vivo* safety and efficacy of an orally-dosed bone-vectored C_{60}-bisphosphonated compound as a therapeutic agent to prevent and treat osteoporosis.

Hydrophilic bisphosphonate groups are known to possess high affinity for the main bone mineral hydroxyapatite. Thus, functionalization of C_{60} with bisphosphonate groups should lead to bone-vectored, water-soluble C_{60} derivatives. Previously developed $C_{60}[C(PO_3H_2)_2]_2$ was administered orally in a rat model of osteoporosis for eight weeks in two separate Experiments at doses of 1 mg/kg and 2.5 mg/kg, respectively. These studies demonstrated that $C_{60}[C(PO_3H_2)_2]_2$ is safe in the rat model: no significant behavior changes occurred, weight gains were normal, and no significant pathology was noted in either the kidney, the liver or the esophagus of the animals. Micro-CT and DXA studies showed significant and positive changes in the bone architecture of the treated

ovariectomized animals which proved, for the first time, that C_{60}-derivatives can be absorbed by the digestive tract and therefore that C_{60}-based scaffolds can be used for oral drug delivery. Just as significantly, the studies also showed that $C_{60}[C(PO_3H_2)_2]_2$ effectively targets bone, making the compound the first example of an *in-vivo* tissue-targeted C_{60}-based drug.

The second part of this work is dedicated to the synthesis and characterization of a beta-blocker conjugate of $C_{60}[C(PO_3H_2)_2]_2$ as a new targeted therapy for osteoporosis. The sympathetic nervous system of mice mediates bone resorption through β_2-adrenergic receptors on bone cells. Thus, the blockage of these receptors could prevent or treat osteoporosis. A non-selective beta-blocker, levobunolol, has been successfully linked to a malonate through a hydrazone formation and then coupled to a C_{60} via Bingel chemistry. Finally, the beta-blocker malonate compound has been also successfully coupled to $C_{60}[C(PO_3H_2)_2]_2$ to form the final target compound, a C_{60}-Bisphosphonate-Beta-blocker conjugate as a new targeted therapy for osteoporosis.

ACKNOWLEDGEMENTS

I wish to thank my research advisor Professor Lon J. Wilson for support, optimism and flexibility. I am grateful to have been part of his group for the last five years.

I thankfully acknowledge Dr. Catherine Ambrose and Dr. Robert Hauge for serving on my thesis committee. I would also like to thank Dr. Catherine Ambrose for a wonderfully productive collaborative experience.

Thanks also go to current and former Wilson group members for support and assistance along the way. I wish to especially thank Dr. Yuri Mackeyev and Dr. Tatiana Zakharyan with whom I not only enjoyed scientific discussions but with whom I also developed beautiful friendships.

I would also like to acknowledge the Robert A. Welch Foundation (Grant C-627) for financial support.

Finally, I dedicate this work to my two sets of parents: Osvaldo and Isabel, and Carolyn and Kenny. One set bought me the boat, and the other taught me how to sail.

TABLE OF CONTENTS

LIST OF FIGURES

LIST OF TABLES

Abbreviations and Symbols

AMBP	ethyl 2-amino-4,4-bis(diethoxyphosphoryl)butyrate
ATP	adenosine-5′-triphosphate
β	beta
Boc_2O	di-tert-butyl dicarbonate
BVF	bone volume fraction
CCl_4	carbon tetrachloride
CBr_4	carbon tetrabromide
CH_2Cl_2	dichloromethane
DBU	1,8-Diazabicyclo[5.4.0]undec-7-ene
DCC	N,N′-Dicyclohexylcarbodiimide
DIPEA	di-isopropyl-ethyl amine
EtOAC	ethyl acetate
FDA	Food and Drug Administration
g	gram(s)
HPLC	High Performance Liquid Chromatography
MALDI-TOF MS	matrix-assisted laser desorption ionization time-of-flight mass spectrometry (spectrum)
mL	milliliter(s)
mmol	millimole
mol	mole
NIH	National Institute of Health

OVX	ovariectomized
PEG	poly(ethylene glycol)
SHM	sham
TMD	total mineral density
WHO	World Health Organization

INTRODUCTION

With the increasing popularity of nanotechnology, scientists have been driven by the need to functionalize and fine-tune nanoparticle properties, including those for fullerenes. C_{60}, the most representative and abundant of the fullerenes in terms of natural ocurrence, possesses unique physical and chemical properties that may be exploited for a wide variety of applications ranging from chemical sensors to superconductivity.[1-5] On the other hand, medical applications for C_{60} were initially avoided because of its poor solubility in biological media. This limitation was soon overcome, however, by chemical derivation of the fullerene cage to produce exo and endohedral fullerene materials that were hydrophilic with substituents such as -OH, $-NH_2$ and -COOH to provide some control over solubility and biological activity.[6, 7]

In the biological arena, experimental results suggested that C_{60} could penetrate cells and cross the blood–brain barrier.[8] Derivatives of C_{60} have shown extraordinary promise as neuroprotective agents,[9] HIV-1 protease inhibitors,[10] photodynamic cancer therapeutics,[11] medical contrast agents and radiotracers,[12, 13] slow-release systems for liposome aerosol delivery,[14] immunotherapy agents,[15] transfection vectors[16] and osteoporosis therapeutics.[17, 18]

Neuroprotective Agents

C_{60} is a powerful oxidizing agent, which makes C_{60}-based compounds potential agents for treating neurodegenerative disorders such as Parkinson's and Alzheimer's diseases which are triggered by the excessive production of superoxide and nitric oxide radicals, presumably due to the over-excitation of glutamic acid receptors.[19] As a result, a

water-soluble malonic acid derivative of C_{60}, known as C_3, (Figure 1) has shown efficacy against excitotoxic necrosis of cultured cortical neurons induced by exposure to glutamate receptor agonists, when administered daily to a mouse model for familial amyotrophic lateral sclerosis. The transgenic mice showed delayed onset of symptoms, improved functional performance, and delayed death as compared with saline-treated controls.[9]

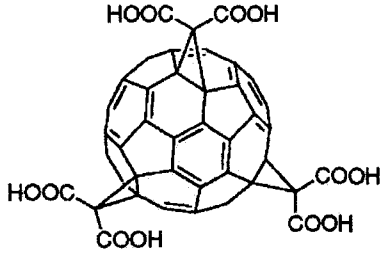

Figure 1. Structure of the C_{60}-malonic acid *e,e e*-$C_{63}(CO_2H)_6$ (C_3).

HIV-1 Protease Inhibitors

HIV protease (HIVP) is a fundamental enzyme for the survival of the human immunodeficiency virus; therefore its inhibition has been the primary goal as a potential therapy for the cure of AIDS. The enzyme active site is an open-ended cylinder which is lined almost entirely by hydrophobic amino acids.[10] In 1993, Friedman et al., realizing that C_{60} has approximately the same radius as the cylinder formed by the active site of the HIVP, demonstrated that C_{60}-derivatives (Figure 2) could block the active site and thereby act as HIVP inhibitors. The positively-charged groups on these new C_{60}-derivatives established electrostatic interactions with the aspartic acids Asp 25 and Asp 125 at the active site setting off its inhibition. The steric and chemical complementaries betweeen the active site of HIVP and C_{60} led scientists to improve the interaction to

obtain optimal EC_{50} (half maximal effective concentration) values of between 0.2 and 1μM.[20]

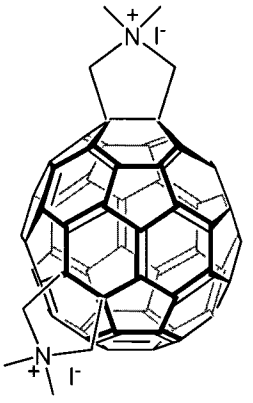

Figure 2. Structure of the alkylated C_{60}-bis (N,N-dimethylpyrrolidinium iodide) derivatives (8 possible geometrical isomers).

Photodynamic Cancer Therapeutics

C_{60} is efficiently converted to its triplet excited state upon UV and visible irradiation making it an attractive candidate for photodynamic therapy. This triplet state efficiently sensitizes the formation of $^1O_2$ in nonpolar solvents and hydroxyl radicals $^{\bullet}OH$ in water, both of which are capable of cleaving DNA.[21] This has been studied using animal microbial cell lines (Salmonella) and plasmids (pBr322) where fragmentations of the DNA and RNA filaments were observed.[11] Conjugations of fullerene with molecular fragments that interact with DNA as intercalators have been performed, increasing the affinities with the nucleic acids. Boutorine et al. synthesized a compound bearing a short oligonucleotide chain (Figure 3) able to interact either with a single filament or with a double chain, forming a duplex or triplex, respectively, following the same process of antisense nucleotides.[22]

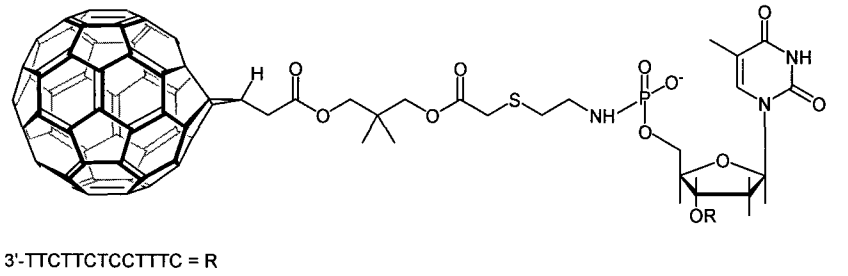

Figure 3. Structure of the C_{60}-oligonucleotide conjugate.

The ability of C_{60} and its derivatives to induce DNA cleavage upon irradiation results in their cytotoxicity both *in-vitro* and *in-vivo*. A C_{60}-carboxylic acid derivative was shown to inhibit proliferation of HeLa S3 cells after two hours of irradiation, while no measurable activity was observed in the dark.[11] In another study, when tumor-bearing mice were treated with a C_{60}-PEG conjugate and subsequently irradiated with visible light, tumor necrosis was induced and when the conjugate was administered at a dose of 8.48 μg/mouse, all tumors were completely ablated.[23]

Medical Contrast Agents and Radiotracers

Current therapeutics containing chelated metal radioisotopes have the disadvantage of kinetic instability *in-vivo*, which can lead to the release of small quantities of toxic radiometals. However, when the toxic radiometal is trapped inside a C_{60} cage it cannot be released. Such metallofullerene species, with metal ions trapped inside the fullerene cage, are called endohedral metallofullerenes and are abbreviated $M@C_{2n}$. Because of their high resistance to metabolism and high kinetic stability, endohedral metallofullerenes represent a unique alternative to metal chelate compounds.

Among endohedral metallofullerenes $Gd@C_{60}[C(COOH)_2]_{10}$ has been shown to be a powerful contrast agent in magnetic resonance imaging (MRI), with a proton

relaxivity greatly exceeding clinical Gd(III) chelate-based MRI agents.[12] In addition, $^{166}Ho@C_{82}(OH)_x$ demonstrated the feasibility of using endohedral metallofullerenes as radiotracers *in-vivo*.[13]

Slow Release System for Aerosol Liposome Delivery

Since systemic chemotherapy has shown little success in the treatment of lung cancer, liposome aerosol delivery of chemotherapeutics directly into the lungs is a desirable alternative treatment for the disease. This therapy employs a variety of lipophilic chemotherapeutics, but unfortunately these drugs are rapidly cleared from the lungs after cessation of aerosol delivery. The hydrophobicity and chemical versatility of C_{60} inspired the synthesis of a C_{60}-paclitaxel conjugate (Figure 4) which demonstrated that once introduced into a liposome formulation it possessed significant anticancer activity in tissue culture.[14]

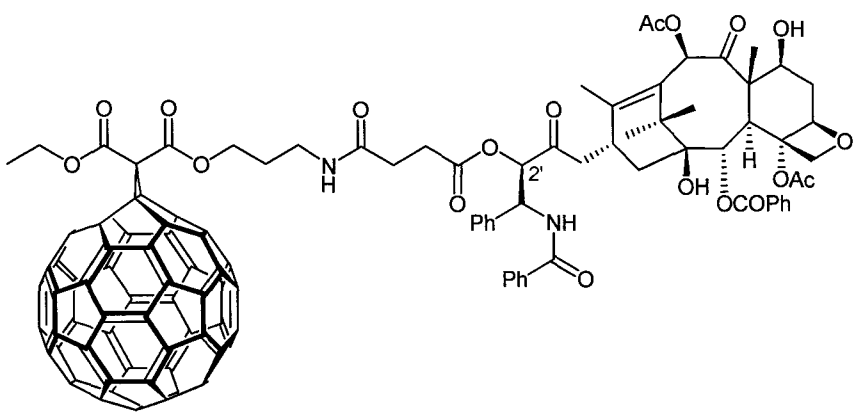

Figure 4. Structure of the C_{60}-paclitaxel conjugate.

Immunotherapy Agents

Immunoconjugates (antibodies conjugated to a second molecule) containing the antibody ZME-018 are rapidly internalized into melanoma cells *in-vitro* and *in-vivo*. A C_{60} water-soluble derivative (Figure 5) has been shown to couple to the ZME-018 antibody and hence has provided the initial step toward targeted fullerene-immunotherapy (FIT).[15]

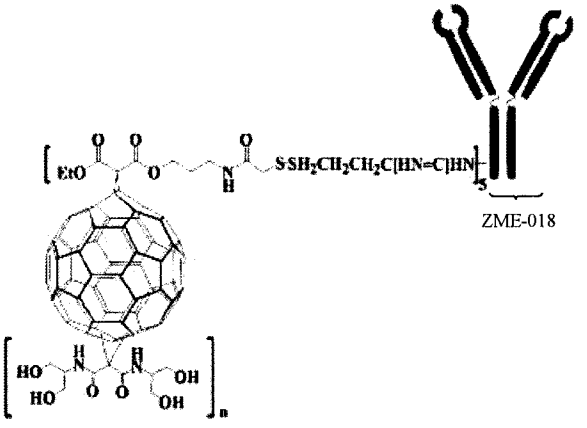

Figure 5. The Structure of the C_{60}-SPDP-(ZME-018) immunoconjugate (C_{60} and antibody figures not to scale).

Transfection Vectors

The specific shape and hydrophobicity of C_{60} results in the ability of certain C_{60} derivatives to mediate gene transfer. Several C_{60}-derivatives were reported to have transfection efficiency comparable to that of the commercially available transfection vectors and a unique ability to sustain protein expression over an extended period of time.[24] In a recent study, a number of positively-charged Prato and Bingel C_{60}-derivatives (Figure 6) have been synthesized and although all of them were positively-charged and therefore were expected to bind DNA, only Bingel bisadducts permitted effective gene

delivery in HEK293 cells.[16] The comparison of the structures of all the C_{60}-derivatives known to permit effective gene delivery reveal similar structural features which include at least four positive charges and a flexible linker between the fullerene core and the amino groups.

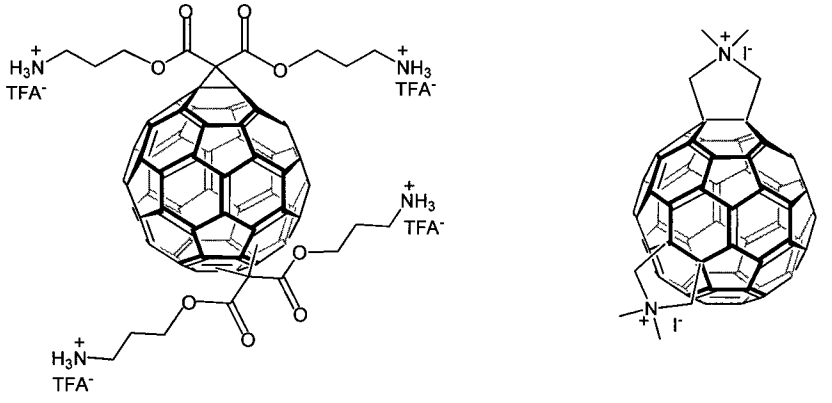

Figure 6. Structures of positively-charged Bingel and Prato C_{60}-derivatives.

Osteoporosis Therapeutics

Bone tissue is an attractive target for vectored therapeutics because its primary inorganic component, hydroxyapatite (HAP), offers a multitude of binding sites. Bisphosphonates, being analogs of naturally-occurring pyrophosphates, are powerful inhibitors of bone resorption and comprise the principal therapy for osteoporosis.[25]

A tissue-vectored bisphosphonate fullerene, $C_{60}(OH)_{16}$AMBP, designed to target bone tissue has been synthesized and evaluated *in-vitro*.[17] However, the synthesis was a multi-step, low yield procedure, and a more convenient, one-step synthesis resulted in the formation of the water soluble C_{60}-bisphosphonate compound $C_{60}[C(PO_3H_2)_2]_2$ (Figure 6).[18] The *in-vivo* oral safety and efficacy of this bone-vectored fullerene is investigated in Chapter I of this Dissertation, and the synthesis and characterization of a beta-blocker

conjugate of $C_{60}[C(PO_3H_2)_2]_2$ as a new targeted therapy for osteoporosis is presented in Chapter II.

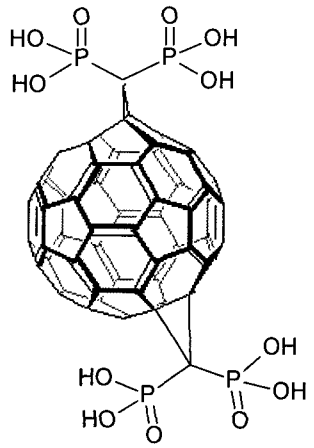

Figure 7. The water-soluble C_{60}-bis(bisphosphonate) compound (8 possible geometrical isomers).

CHAPTER I

In-vivo TESTING OF A BONE-SELECTIVE C_{60} FULLERENE: SAFETY AND EFFICACY TESTING

INTRODUCTION

Structure and Biological Activity of Bisphosphonates

The discovery of bisphosphonates is regarded as a milestone in the history of osteoporosis. Bisphosphonates (Figure 7) are synthetic, non-hydrolyzable analogues of naturally occurring pyrophosphate but contain a carbon atom in place of oxygen, which allows structural variations. Since their development, bisphosphonates have been used to treat Paget's disease,[26] hypercalcemia,[27] osteoporosis,[28, 29] and breast cancer.[30, 31] Bisphosphonates are antiresorptive agents, which mean they slow or stop the natural process that dissolves bone tissue. This results in maintained or increased bone density and strength which may prevent the development of osteoporosis.

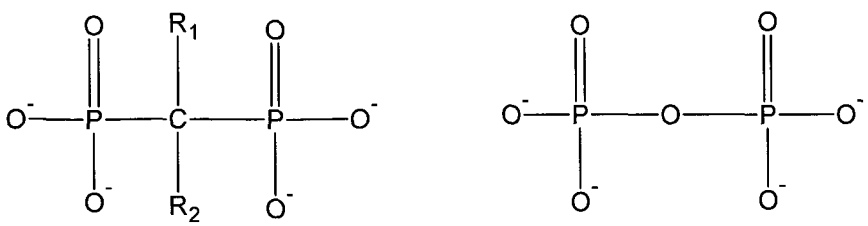

Figure 8. Structure of bisphosphonate and pyrophosphate.

Bisphosphonates form a three-dimensional structure capable of chelating divalent ions such as Ca^{2+}, Mg^{2+}, and Fe^{2+}. [32] Ca^{2+} binds more effectively if one side chain (R_1) is an –OH or an $–NH_2$ group.[33] The R_2 side chain may influence potency and mineral binding, i.e. longer R_2 side chains increase potency and bulky R_2 side chains have a lower

affinity for bone mineral. Several bisphosphonates containing a secondary amine group in the R_2 side chain have also been found to be more potent than those containing a primary amine. Bisphosphonates containing an –OH group as the R_1 side chain and a tertiary nitrogen within a ring structure in the R_2 side chain appear to be the most potent antiresorptive bisphosphonates discovered to date.[34, 35]

There are two classes of bisphosphonates, simple bisphosphonates and nitrogen-containing bisphosphonates, which differ in the role they play toward osteoclasts (bone-resorbing cells). The simple bisphosphonates are incorporated into analogues of ATP that accumulate in osteoclasts, resulting in initiation of osteoclasts apoptosis.[36] On the other hand, nitrogen-containing bisphosphonates inhibit the enzyme farnesyl diphosphate synthase (FPP) which plays a role in the cholesterol synthesis pathway. As a result, there is a reduction in the lipid geranyl diphosphate, which prenylates GTPases leading to osteoclast inactivation.[37, 38]

Although they are poorly absorbed orally (less than 10%), both classes of bisphosphonates have a high affinity for hydroxyapatite crystals and deposit at bone turnover sites. Since the P-C-P group is resistant to enzymatic hydrolysis, only nitrogen-containing bisphosphonates are not metabolized and are excreted by the kidneys unchanged. They are pharmacologically characterized by their ability to inhibit bone resorption, and pharmacokinetically by their similarities in absorption, distribution and elimination.

Bisphosphonates are considered to be safe, and long-term treatment has not shown a risk for serious adverse effects or death.[39] However, if not taken properly, oral bisphosphonates can cause upper gastrointestinal effects, and intravenously

bisphosphonates may cause influenza-like illness/acute-phase reactions, renal impairment and rarely osteonecrosis of the jaw.[39]

Targeting Strategies for Bisphosphonates

A variety of compounds (rofecoxib, valdecoxib, estrogen, parathyroid hormone, etc.) have been identified that benefit many bone diseases, but they are not well tolerated when delivered systemically due to deleterious effects on other tissues; therefore, the need to target bone tissue is of significant importance. This is where bone-targeting with bisphosphonates offers hopeful results. When alendronate, the most common bisphosphonate on the market, was administered intravenously to rats, about 60%-70% of the dose was found in bone within one hour and this remained unchanged 71 hours later.[40] This finding offered a promising bone-targeting approach that has been widely studied.

Previous work in our laboratories demonstrated that the addition of a bisphosphonate group to C_{60} to create the C_{60}-bisphosphonate derivative, $C_{60}(OH)_{16}AMBP$, targeted the molecule selectively to bone.[17] *In-vitro* experiments demonstrated that the C_{60}-bisphosphonate derivative had a similar mechanism of action as other commercially-available bisphosphonate drugs. In a follow-up study, another C_{60}-bis(bisphosphonate) derivative, $C_{60}[C(PO_3H_2)_2]_2$, was synthesized and thoroughly characterized.[18]

The development of animal models in osteoporosis is an interesting and valuable approach to understanding the pathophysiological mechanism of bone loss; in addition, such models can be used to test the efficacy of new therapeutic strategies. The

ovariectomized (OVX) rat is considered by the WHO and the FDA as the most suitable model of post menopausal osteoporosis.[41] In this study, $C_{60}[C(PO_3H_2)_2]_2$ has been tested *in-vivo* in order to determine the safety of long-term oral dosing and to investigate whether the test compound affected bone tissue after oral dosing in rats when administered at two different doses.

Two experiments with two doses were conducted *in-vivo* at two different times. The first experiment used a dose of 1mg/kg which was based on a commonly used dosage for alendronate with the main intent being an evaluation of the *in-vivo* safety of the drug when dosed orally. A second experiment followed, at a dose of 2.5mg/kg, which produced a more favorable efficacy result. Since this compound has not been previously tested in animals, the main concern was the safety of oral dosing. Ovariectomized and sham-operated animals were dosed orally with the test compound for eight weeks. The microarchitecture of the bone was analyzed, and the pathology of the liver, kidney and esophagus investigated.

EXPERIMENTAL

Materials and Methods

C_{60} (>99%) was purchased from MER Corporation (Tucson, Arizona) and used without further purification. All solvents were reagent grade. CCl_4 was dried over P_2O_5. Tetraisopropyl bromomethylenediphosphonate was prepared according to the method of McKenna from tetraisopropyl methylenediphosphonate.[42] All reactions were performed under inert gas atmosphere.

Experiment 1

Eighteen female retired breeder Sprague Dawley (SD) rats, approximately nine months of age, were purchased from Harlan (Indianapolis, IN). The original mean body weight of these animals was 289 grams. The rats were acclimated for one week under standard laboratory conditions, had free access to water, and were fed a standard rat chow (Teklad, Harlan). All animal procedures were performed under the guidelines of the University of Texas Health Science Center at Houston animal care and use committee in compliance with the *NIH Guide for the Care and Use of Laboratory Animals*. Animals were anesthetized using isoflurane inhalant titrated to effect. All animals received one injection of buprenorphine for pain (0.01mg/kg) prior to incision. Ovariectomies were performed via a standard dorsal incision. In the sham-operated groups, both ovaries were identified but left intact. The skin incision was then closed with nonresorbable sutures.

The animals were divided into three equal groups: ovariectomized untreated (OVX1-control), ovariectomized treated (OVX1-treated), and sham-operated treated (SHM1-treated). The treated animals were dosed three days per week by oral gavage with the test compound, $C_{60}[C(PO_3H_2)_2]_2$, with a dose of 1mg/kg.

Experiment 2

To follow up with the results obtained from Experiment 1, a second set of nineteen female retired breeder Sprague Dawley (SD) rats, approximately nine months of age, were purchased from Harlan (Indianapolis, IN). The original mean body weight of these animals was 323 grams. Animal procedures, care, ovariectomies and operations were performed as described in Experiment 1.

The animals were divided into the following groups: ovariectomized untreated (OVX2-control), ovariectomized treated (OVX2-treated), and sham-operated treated (SHM2-treated). For this experiment the treated animals were dosed three days per week by oral gavage with the test compound, $C_{60}[C(PO_3H_2)_2]_2$, with a dose of 2.5mg/kg.

In both experiments, all animals were treated for eight weeks before sacrifice. Activity levels, food and water intake, and weight gain were monitored to determine gross tolerance to the drug.

At the termination of the study, all animals were euthanized by exsanguination under anesthesia. The femora were removed and stripped of soft tissues for either micro-CT analysis or plastic embedding for light microscopic analysis. All bones for micro-CT analysis were wrapped in saline-soaked sponges and frozen at -20°C until tested. All bones for plastic embedding were placed in 70% ethanol prior to dehydration and infiltration with the plastic. After polymerization of the plastic, sections were prepared using a cutting and grinding technique. One kidney and one lobe of the liver (chosen randomly) were removed from each animal and placed in 10% neutral buffered formalin for 24 hours and then transferred to 70% ethanol. For Experiment 2, the esophagi were also removed to study pathological changes. These organs were processed using standard paraffin techniques and stained with H&E. A pathologist blinded to the study groups evaluated each section for signs of inflammation, tissue damage, tissue changes, or toxicity.

Synthesis of the Test Compound

$C_{60}[C(PO_3iPr_2)_2]_2$ was prepared as previously described.[18] Flash chromatography on silica gel using chloroform as eluent was used for the preliminary separation. After

removal of the monoadduct as a purple-red colored band, a second dark-amber fraction containing mainly the bisadduct isomers was collected. Further separation was achieved by HPLC on a preparative "Econosil Silica" column with a toluene-methanol mixture (9:1) as eluent to obtain the eight different possible $C_{60}[C(PO_3iPr_2)_2]_2$ isomers. However, for these studies the isomers were not separated. The bis(bisphosphonic) acid, $C_{60}[C(PO_3H_2)_2]_2$, obtained after hydrolysis with $Si(CH_3)_3I$, was converted into its sodium salt by addition of NaOH 0.1 N. The resulting salt was adjusted to pH 7.4 and then dried under vacuum. The desired concentrations of 1 mg/mL and 2.5 mg/mL were then obtained and made 0.9 % isotonic.

***Ex-Vivo* Micro Computed Tomography (Micro-CT)**

Experiment 1

Micro-CT scanning and analysis was carried out with a GE Medical Systems (formerly EVS Corp, London Ontario) Locus RS-9 Micro-CT Scanner. The unit is a cone-beam volume CT system which uses a tungsten source X-ray tube that may operate at 35 to 80 kV and 0.10 to 0.50 mA for scans. In the protocol used for high-resolution images of the rat femurs, 80 kV and 0.45 mA were used. The rat femurs were scanned on the micro-CT unit while still wrapped in wet gauze using the specimen (27 micrometer voxel, 80 minute) scan mode. Between sessions, the bone specimens were frozen at -20 °C in saline-soaked gauze and were sealed in plastic bags. Two femurs were scanned side-by-side in a single pass and were marked for identification.

After the data acquisition phase was completed, the reconstruction software normalized the images based on air projections in order to eliminate detector errors and

standardize the acquired data. All scans were calibrated into proper Hounsfield units (HU) by sampling air and water raw values obtained from scanning a small tube of water prior to beginning the specimen scan acquisitions. After the 3D volume reconstruction and reorientation was complete, the femurs were analyzed using software provided by the scanner manufacturer (MicroView ^{TM}).

The distal cancellous region of interest for stereology measurements was defined as originating 0.5 mm proximal to the distal growth plate with depth fixed at 3 mm (away from the growth plate). Morphologic characteristics were calculated in the three orthogonal planes and then averaged. This sampling analysis calculated multiple parameters of the cancellous bone: Bone Volume/Total Volume (BV %), bone surface/bone volume (BS/BV), trabecular thickness (TbTh), trabecular number (TbN), and trabecular spacing (TbSp) based on a standardized threshold for bone (1000 HU). In addition, bone mineral content (BMC) and density (BMD) were calculated for the distal region.

Experiment 2

Micro-CT scanning and analysis was carried out using a GE Medical Systems (formerly EVS Corp, London Ontario) Locus SP Micro-CT Scanner. The unit is a flat panel, cone-beam scanner suitable for *ex-vivo* imaging at high resolutions. It uses a tungsten source X-ray tube that may operate at 50 to 90 kV. The rat femurs were scanned on the micro-CT unit while still wrapped in wet gauze using the specimen (27 micrometer voxel, 80 minute) scan mode. Between sessions, the bone specimens were frozen at -20 °C in saline-soaked gauze and were sealed in plastic bags. Two femurs were scanned side-by-side in a single pass and were marked for identification.

As in Experiment 1, after the data acquisition phase was completed, the reconstruction software normalized the images based on air projections in order to eliminate detector errors and standardize the acquired data. All scans were calibrated into proper Hounsfield units (HU) by sampling air and water raw values obtained from scanning a small tube of water prior to beginning the specimen scan acquisitions. After the 3D volume reconstruction and reorientation was complete, the femurs were analyzed using software provided by the scanner manufacturer (MicroView ^{TM}).

The three following regions were studied: the midshaft of the femur, the distal femur proximal (regular) to the growth plate and the distal femur distal (ultradistal) to the growth plate. These sampling analyses calculated multiple parameters of the cancellous bone: Bone Volume/Total Volume (BV%), bone surface/bone volume (BS/BV), trabecular thickness (TbTh), trabecular number (TbN), and trabecular spacing (TbSp) based on a standardized threshold for bone (1000 HU). In addition, bone mineral content (BMC) and density (BMD) were calculated for the regular and ultradistal region.

Bone Densiometry

The right femurs of all animals from Experiment 2 were cleaned of soft tissue and scanned with a Hologic QDR 4000 DXA in a container of water. The Regional High Resolution software of the instrument was used to divide the femur into four equal segments based on the length of each femur (Figure 9), L1 to L4. The femoral scan images were obtained, and bone area, BMC, and BMD of the whole femur and of distal femur (near the knee) (L1), femoral shaft (L2 and L3) and proximal femur (near the hip) (L4) were determined, as were the ultradistal, which is the bottom $1/6^{th}$ of the femur, and

the ultra proximal from top of great trochanter to most prominent point of lesser trochanter.

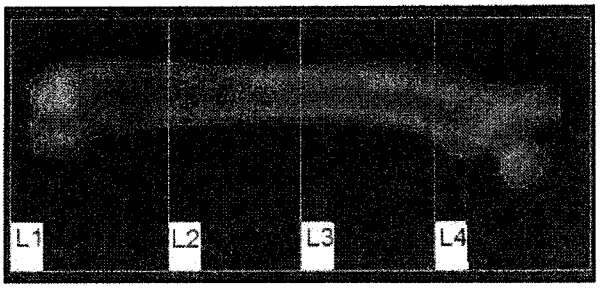

Figure 9. Image of femur obtained with a Hologic QDR 4000 DXA.

Statistical Analysis

All measures except the pathology findings were analyzed using ANOVA. If significant differences were found, post-hoc analysis was performed using Tukey's Honestly Significant Differences. P values of less than 0.05 were considered significant.

RESULTS AND DISCUSSION

Gross Tolerance of $C_{60}[C(PO_3H_2)_2]_2$

Animals from both experiments dosed with the test compound tolerated the treatment without signs of distress or toxicity. In Experiment 1, the weight gain was an average of 46.4g for the OVX1-control group, 31.1g for the OVX1-treated group, and -5.5g for the SHM1-treated group; whereas, in Experiment 2 the weight gain was more prominent with values of 65.3g for the OVX2-control group, 44.8g for the OVX2-treated group, and 17.2g for the SHM2-treated group. These values indicate no apparent effect of long-term treatment with $C_{60}[C(PO_3H_2)_2]_2$. In addition to normal weight gain, all animals demonstrated normal activity levels, food and water intake, and grooming habits.

Kidney and Liver Pathology Results

Kidney and liver sections of all animals demonstrated that all findings were within normal limits. Some of the sampled liver tissues had non-specific morphologic features that are found in a variety of physiologic and pathophysiologic changes in the liver. These changes include portal lymphocytic infiltrates, focal spotty necrosis (hepatocytolysis), and microvesicular fatty changes. These findings were so minimal and localized that they were thought to be physiologically normal and not related to any major toxic, metabolic, neoplastic, or infectious event. In Experiment 1, 4 out of 6 animals from the OVX1-control, 3 out of 6 animals from the OVX1-treated, and 5 out of 6 animals from the SHM1-treated group demonstrated these findings. Whereas, in Experiment 2, 1 out of 6 animals from the OVX2-control, 3 out of 7 animals from the OVX2-treated, and 6 out of 6 animals from the SHM2-treated groups also showed these changes in the liver. All kidneys were without significant histopathologic changes and the inflammation found in some of the tissues was consistent with abdominal surgery. Microscopically, all livers and kidneys were reported to be healthy and viable. In Experiment 2, the sampled esophagi showed esophagitis in 4 out of 6 animals from the OVX2-control, 3 out of 7 animals from the OVX2-treated, and 5 out of 6 animals from the SHM2-treated groups. Since all animals were dosed using oral gavage and esophagitis is present in all groups it is difficult to separate drug from gavage effect.

Micro-CT Analysis

Experiment 1

In nearly all parameters measured using Micro-CT, the mean value for the OVX1-treated group was between the OVX1-control and the SHM1-treated (Table 1). All p-values from ANOVA analysis are given, and a p-value less than 0.05 was taken to demonstrate a significant difference between the groups. If a dose of 1mg/kg of the test compound had proven to be an efficacious treatment, then we would have expected the OVX1-treated group to be significantly different from the OVX1-control but not from SHM1-treated. In most measures where a significant difference was detected between the groups, the OVX1-treated group was not significantly different from the OVX1-control group, but was significantly different from the SHM1-treated group. For measures marked by an asterisk, the homogeneous subset analysis demonstrated that OVX-treated was not significantly different from either OVX-control or SHM-treated, although these groups were significantly different from each other. These results may indicate that the treatment had an effect but that the dosage was too low to have a significant effect. Therefore, Experiment 2 was performed with the hope of achieving better results.

To investigate the effect of $C_{60}[C(PO_3H_2)_2]_2$ on the sham-operated animals, we compared the micro-CT values from the SHM1-treated group to sham-operated animals from a previous study.[43] No significant differences were detected (data not shown here), indicating that the compound did not have a significant effect on the sham-operated animals.

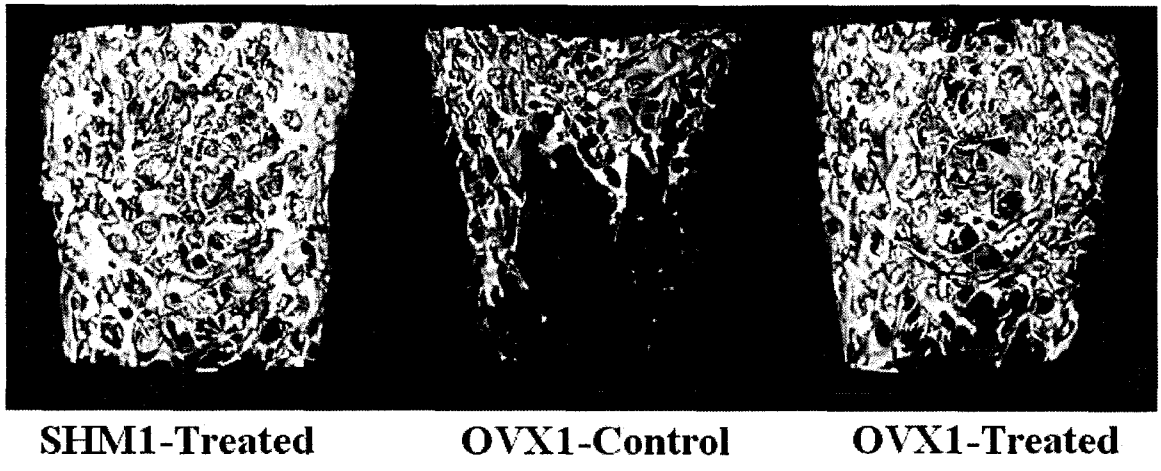

Figure 10. Representative micro-CT images for animals of Experiment 1 after eight weeks of dosing with the test compound, $C_{60}[C(PO_3H_2)_2]_2$.

Table 1. Experiment 1 micro-CT data.

Micro-CT Measure	OVX1-control	OVX1-treated	SHM1-treated	ANOVA p-value
BV%	3.77 (1.82)	4.63 (1.53)	8.55 (4.91)	0.043 *
BSBV	43.37 (4.80)	41.53 (5.26)	31.27 (5.34)	0.002
TbTh (μm)	46.65 (5.39)	48.87 (6.82)	65.48 (11.11)	0.002
TbN	0.79 (0.39)	0.95 (0.30)	1.29 (0.61)	NS (0.188)
TbSp (μm)	1460.67 (639.18)	1126.33 (487.42)	892.67 (481.13)	NS (0.221)
BMC (mg)	7.05 (1.47)	8.56 (1.27)	8.28 (1.92)	NS (0.133)
BMD (mg/cc)	213.00 (49.59)	240.83 (31.05)	272.95 (55.54)	NS (0.117)
TMC (mg)	2.41 (0.83)	3.20 (0.71)	4.08 (1.61)	NS (0.063)
TMD (mg/cc)	669.45 (23.43)	679.14 (20.71)	685.08 (26.13)	0.026 *
BVF	0.11 (0.04)	0.13 (0.02)	0.17 (0.06)	NS (0.062)
Calib TbTh 3D (μm)	59.34 (10.15)	65.86 (6.02)	76.18 (10.49)	0.009 *
Calib TbSp 3D (μm)	2015.53 (188.81)	1693.51 (278.21)	1722.34 (273.96)	NS (0.078)
Euler Volume	17.622 (9.045)	20.21 (6.50)	20.08 (10.26)	NS (0.848)

Experiment 2

In contrast to Experiment 1, in nearly all parameters measured using Micro-CT, the mean value for the OVX2-treated group of Experiment 2 was closer to the SHM2-treated than the OVX2-control (Table 2). As in Experiment 1, all p-values from ANOVA analysis are given, and a p-value less than 0.05 was taken to demonstrate a significant difference between the groups. The BMC and the TMD for the SHM2-treated and OVX2-treated are very close to each other, but significantly different from the OVX2-control group. These results confirm that an increase of dosage was necessary to obtain more favorable results, and to prove that the test compound, $C_{60}[C(PO_3H_2)_2]_2$, has a significant effect.

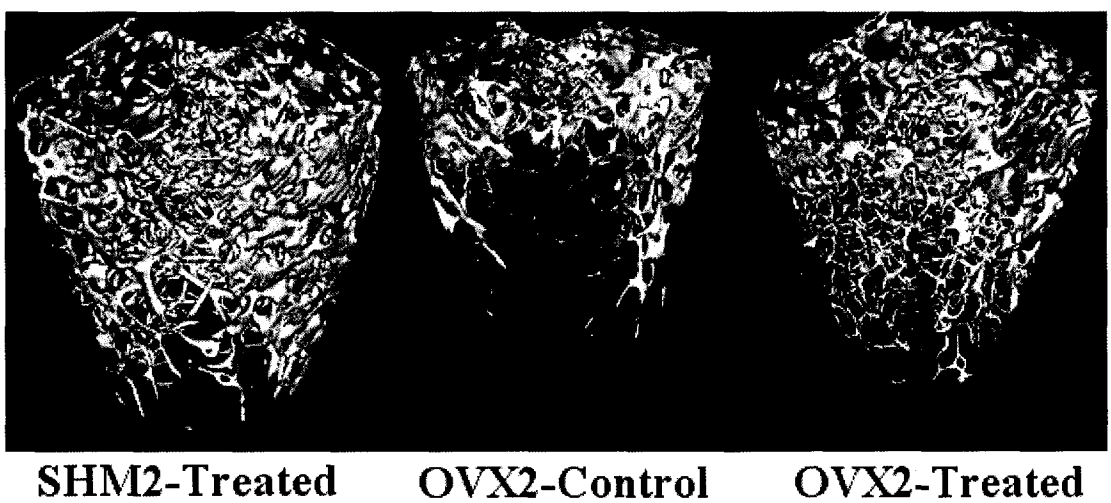

Figure 11. Representative micro-CT images for animals of Experiment 2 after eight weeks of dosing with the test compound, $C_{60}[C(PO_3H_2)_2]_2$.

Table 2. Experiment 2 micro-CT data (regular, ultradistal and midshaft).

Regular

Micro-CT Measure	OVX2-control	OVX2-treated	SHM2-treated	ANOVA p-value
BSBV	30.57 (3.04)	29.11 (3.43)	29.36 (4.34)	NS (0.763)
TbTh (μm)	65.95 (6.56)	69.46 (7.96)	69.39 (10.35)	NS (0.718)
TbN	1.72 (0.36)	1.72 (0.28)	1.73 (0.64)	NS (0.997)
TbSp (μm)	543.96 (162.18)	526.96 (102.32)	565.33 (202.19)	NS (0.918)
BMC (mg)	11.09 (1.06)	11.88 (1.01)	12.27 (2.86)	NS (0.549)
BMD (mg/cc)	297.86 (19.43)	305.27 (29.64)	320.10 (74.10)	NS (0.716)
TMC (mg)	3.72 (0.79)	4.18 (0.80)	4.38 (2.32)	NS (0.741)
TMD (mg/cc)	882.39 (26.56)	900.76 (27.83)	903.92 (32.39)	NS (0.405)
BVF	0.11 (0.02)	0.12 (0.02)	0.13 (0.07)	NS (0.879)
Euler Volume	19.91 (7.05)	15.72 (3.89)	18.20 (9.41)	NS (0.604)

Ultradistal

Micro-CT Measure	OVX2-control	OVX2-treated	SHM2-treated	ANOVA p-value
BMC (mg)	119.61 (8.64)	136.74 (11.06)	138.51 (7.30)	0.005
BMD (mg/cc)	739.35 (69.34)	806.14 (47.51)	795.63 (57.74)	NS (0.142)
TMC (mg)	92.22 (8.14)	106.81 (11.03)	111.31 (7.52)	0.006
TMD (mg/cc)	1036.23 (83.29)	1130.53 (34.02)	1084.44 (79.24)	NS (0.094)
BVF	0.55 (0.02)	0.56 (0.04)	0.59 (0.03)	NS (0.072)
Calib TbTh 3D (μm)	239.14 (18.45)	261.12 (38.48)	279.41 (33.00)	NS (0.114)

Midshaft

Micro-CT Measure	OVX2-control	OVX2-treated	SHM2-treated	ANOVA p-value
Mean Thickness (mm)	0.62 (0.06)	0.60 (0.09)	0.62 (0.07)	NS (0.829)
Inner Perimeter (mm)	7.88 (0.66)	8.47 (0.54)	8.32 (0.47)	NS (0.202)
Outer Perimeter (mm)	11.78 (0.41)	12.13 (0.24)	12.31 (0.32)	0.040
Marrow Area (mm^2)	4.63 (0.74)	5.33 (0.68)	5.20 (0.66)	NS (0.207)
Cortical Area (mm2)	5.87 (0.42)	5.91 (0.61)	6.15 (0.62)	NS (0.730)
Total Area (mm2)	10.50 (0.66)	11.24 (0.58)	11.34 (0.48)	0.044
BMD (mg/cc)	1428.07 (29.66)	1489.49 (52.61)	1477.16 (32.90)	0.040

Femoral Bone Mineral Density

The effects of ovariectomies and treatment with $C_{60}[C(PO_3H_2)_2]_2$ on the BMD of the right femur measured by DXA are shown in Table 3. The mean BMD values for the OVX2-control group at L1(distal femur) and at the ultradistal trochanter were significantly lower than those for the SHM2-treated group, which indicated an ovariectomy-induced decrease in BMD in these areas. There were no significant changes observed in L2 (mid-shaft distal) and L3 (mid-shaft proximal) BMD in the OVX2-control relative to the values of SHM2-treated. The mean BMD value at L4 (proximal femur) of the OVX2-control was lower but not significantly lower than that for the SHM2-treated, and the BMD value of the OVX2-treated was significantly higher than that for the OVX2-control which proved that $C_{60}[C(PO_3H_2)_2]_2$ inhibits the loss in BMD at L4.

Table 3. DXA data for Experiment 2.

DXA Measure	OVX2-control	OVX2-treated	SHM2-treated	ANOVA p-value
Dist femur BMD (L1)	0.2413 (0.0068)	0.2480 (0.0211)	0.2654 (0.0130)	0.035
BMD2 (L2)	0.2175 (0.0090)	0.2095 (0.0167)	0.2150 (0.0131)	NS (0.574)
BMD3 (L3)	0.2640 (0.0108)	0.2661 (0.0215)	0.2545 (0.0253)	NS (0.582)
Prox Femur BMD (L4)	0.2508 (0.0090)	0.2600 (0.0246)	0.2531 (0.0143)	NS (0.638)
Ultradistal BMD	0.2703 (0.0064)	0.2812 (0.0258)	0.3024 (0.0121)	0.015
Ultraproximal BMD	0.2527 (0.0089)	0.2635 (0.0241)	0.2574 (0.0143)	NS (0.555)

Discussion

Tissue-targeted drug-delivery systems offer localized treatment without significant systemic effects. For some years, tetracycline and its analogs were linked to various drugs to increase their affinity to bone.[44-46] For mineralized tissue, bisphosphonates offer promise as a delivery vehicle as these compounds have a high

affinity for bone.[47,48] Several laboratories are investigating methods of using bisphosphonates as part of a bone-targeted drug delivery system.[49-52] Uludag and coauthors have been investigating protein-based therapeutic agents by modifying the protein with bisphosphonates.[50] Their *in-vitro* and *in-vivo* studies have demonstrated that this approach has great promise. Wang et. al., have developed water-soluble drug delivery systems using poly(ethyleneglycol) and poly[N-(2-hydroxypropyl) methacrylamide].[53] *In-vitro* and *in-vivo* data also demonstrated that these delivery systems can accumulate in bone tissue.

In this study, we have investigated the *in-vivo* safety and efficacy of a fullerene (C_{60})-based bisphosphonate compound as a bone-targeted drug delivery platform. Before performing future *in-vivo* work, the present study was undertaken to evaluate the safety of the present bisphosphonated C_{60} compound in rats and also to establish the relative potency of the test compound compared to other bisphosphonate drugs which are currently commercially-available, such as alendronate and etidronate. For our study, two experiments at different doses were performed. A dose of 1mg/kg was chosen for Experiment 1 based on previous studies of alendronate in rats to primarily investigate the safety of the compound in rats after oral dosing. In addition, a dose of 2.5mg/kg was chosen for Experiment 2 to study the efficacy developments after dosage increase. Experiment 1 results demonstrated some positive changes in the treated ovariectomized animals with respect to the untreated animals, but the results were not always significant. However, the test compound proved to be safe after eight weeks of oral dosing. The increase of dosage in Experiment 2 proved to be necessary and showed additional

significant and encouraging results. Still, higher doses of the compound may be necessary to find an optimum dose and to improve the observed efficacy of Experiment 2.

Nevertheless, the present results do conclusively demonstrate that the C_{60}-bis(bisphosphonate) test compound, at these doses, is safe in the rat model. No significant behavior changes were noted over the eight-week studies. In addition, weight gains were normal, and no significant pathology was noted in the kidney, liver or esophagus of the animals.

CONCLUSIONS

This study has demonstrated, for the first time, that the orally-administered C_{60}-bis(bisphosphonate) test compound, $C_{60}[C(PO_3H_2)_2]_2$, can be used safely in a rat model of osteoporosis. In addition, the test compound reduced the bone density loss that is usually seen after ovariectomies, although the magnitude of the treatment effect could likely be further improved with higher doses. Our results also prove, for the first time, that C_{60} derivatives can be absorbed by the digestive tract and therefore that C_{60}-based scaffolds can be used for oral drug delivery. Just as significantly, the study has also shown that the test compound effectively targets bone, making the compound the first example of an *in-vivo* tissue-targeted C_{60}-based drug.

CHAPTER II

A C_{60}-BISPHOSPHONATE-BETA-BLOCKER CONJUGATE: A NEW TARGETED THERAPY FOR OSTEOPOROSIS

INTRODUCTION

C_{60} fullerene provides a biologically stable and convenient three-dimensional scaffold for covalent attachment of multiple drugs to create single-dose "drug cocktails." This drug-delivery strategy adds to the growing list of potential biomedical applications for C_{60} derivatives. Since C_{60}-bisphosphonate derivatives have afforded promising results in a rat model for the treatment of osteoporosis as discussed in Chapter I, additional drug molecules attached to the C_{60} core might afford an even better therapeutic agent. Chapter II explores this concept with the synthesis and characterization of the first C_{60}-Bisphosphonate-Beta-blocker conjugate.

Structure and Biological Activity of Beta-blockers

In 2005, Dr. Gerard Karsenty reported that a link exists between leptin, a hormone that regulates appetite and metabolism, and bone remodeling.[54] His group demonstrated that the sympathetic nervous system of mice mediates bone resorption through β_2-adrenergic receptors on bone cells. Thus, blocking the sympathetic nervous system from interaction with these receptors could prevent or treat osteoporosis.

Beta-adrenergic antagonists or beta-blockers comprise a group of drugs that are mostly used to treat cardiovascular disorders such as hypertension, cardiac arrhythmia, or ischemic heart disease. They possess a natural high degree of enantioselectivity in binding to β (β_1 and/or β_2) receptors, and they competitively inhibit the beta effects of

endogenous catecholamines, which are "fight-or-flight" hormones (adrenaline, noradrenaline and dopamine) that the adrenal glands release in response to stress. Because beta-blockers are so active, they cannot be administered systemically for the treatment of osteoporosis. For this reason, if beta-blockers are to be used as a therapy for osteoporosis or other bone disorders, they will need to be targeted and delivered mainly to bone to minimize cardiovascular side effects.[47]

The first beta-blocker, dichloro-isoproterenol, which was introduced in 1958 opened a new era for cardiovascular pharmacotherapy. A few years later, propanolol was approved by the FDA and became the first beta-blocker for clinical use. The development of selective (β_1 or β_2 receptor) beta-adrenergic agonist or antagonist drugs followed shortly thereafter.[47]

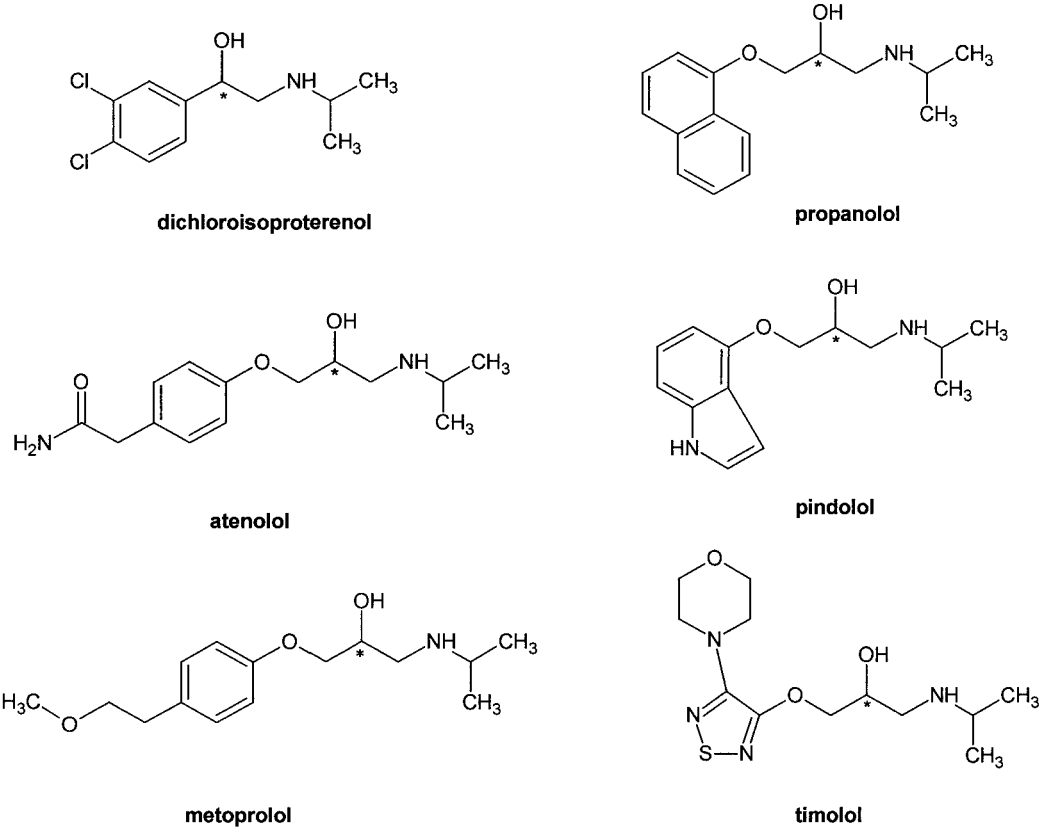

Figure 12. Chemical structures of major beta-blockers (* = chiral center).

Each of the beta-blockers possesses at least one chiral center. In addition, all beta-blockers have at least one aromatic ring structure attached to a side alkyl chain possessing a secondary hydroxyl and amine functional group. The amine has an isopropyl or bulkier substituent group which appears to favor the interaction with beta-receptors.[55] The nature of the substituents on the aromatic ring determines whether the effect will be predominantly activation or blockage.[55] As mentioned above, most of the beta-blockers (e.g., propranolol, metoprolol, atenolol, and pindolol) have one chiral center, and as a result, they are marketed as a racemate of two enantiomers; the exception is timolol which is marketed as an S-enantiomer.[56]

Pharmacologically, beta-blockers are distinguished based on their selectivity for beta-receptors. The non-selective beta-blockers, including propranolol, pindolol, and timolol, block both β_1- and β_2-adrenergic receptors. On the other hand, selective beta-blockers, including metoprolol and atenolol, have greater affinity for β_1 receptors.

In general, beta-blockers are non-stereoselectively absorbed from the gastrointestinal tract via passive diffusion. The lipophilic beta-blockers are eventually metabolized and therefore eliminated. However, the more hydrophilic beta-blockers are usually excreted unchanged in urine.[56]

Structure and Activity of Levobunolol

With all the different chemical structures offered by beta-blockers (Figure 12), a vast list of possibilities existed from which to choose a beta-blocker that could be attached to C_{60}. However, in our design strategy, the potential beta-blocker had to offer a necessary functional group for linkage to a malonate which could then be reacted with

C_{60} via Bingel chemistry.[57] This reaction had to insure that the active site of the beta-blocker would not be compromised. All the beta-blockers have a common alkyl chain with a secondary amine at the active site that favors the interaction with beta-receptors. Thus, this part of the molecule needed to be left intact for the drug to remain active. Most of the beta-blockers differ on the type of aromatic ring and its substituents. Therefore, chemical conjugation with the aromatic ring should still retain drug activity. On the basis of these considerations, levobunolol was chosen as the beta-blocker for this study. Levobunolol has a tetralone structure (Figure 13) which provides a good group for chemical modification and attachment to malonates.

Levobunolol, (-)-5-[3-(tert-Butylamino)-2-hydroxypropoxy]-3,4-dihydro-1(2H)-naphthalenone, is the levorotatory and pharmacologically active isomer of bunolol. It is a potent non-selective beta-blocker which was synthesized by Schwender et al. in 1970 by the reaction of epichlorohydrin with 5-hydroxy-1-tetralone in the presence of NaOH.[58] It is currently marketed as a hydrochloride ophthalmic solution for the treatment of glaucoma as AKBeta® and Betagan®.

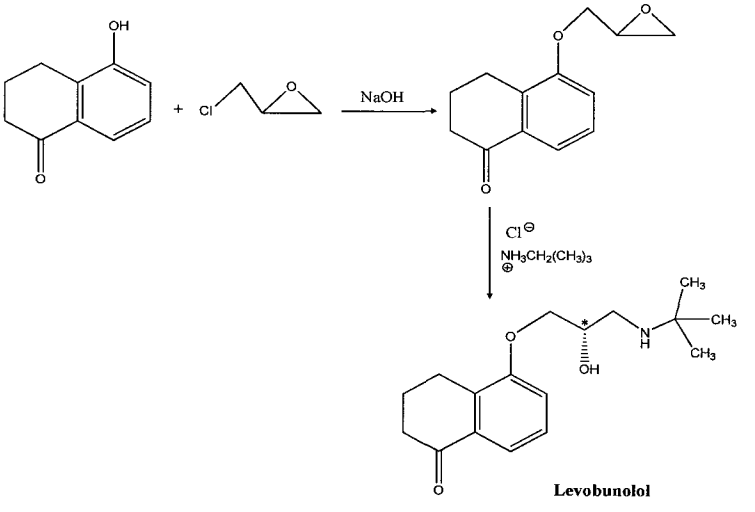

Figure 13. Synthesis and Chemical Structure of Levobunolol (* = chiral center).

Levobunolol's mechanism of action in reducing intraocular pressure is believed to be due to a reduction of the production of aqueous humor via inhibition of adrenergically driven processes within the ciliary processes.[59]

Studies with anesthetized dogs have shown that levobunolol is approximately six times more potent than propanolol by an intravenous route; whereas after oral administration a 45-fold potency difference was observed.[60] It is rapidly absorbed after oral administration with a mean peak plasma concentration occurring between 1 and 3 hours after dosing. It undergoes metabolism through oxidative, reductive and conjugation pathways to yield at least 9 metabolites which account for 55% of the oral dose (dihydrobunolol accounts for 28%), while unchanged levobunolol accounts for only 15%. In humans, about 77% of the dose is excreted by the kidney in the urine and 3% in the feces.[61]

C_{60} as a Targeted Scaffold for Drug Delivery

In this work, the first use of C_{60} as a "drug cocktail" for the treatment of osteoporosis has been accomplished by the design and synthesis of a C_{60}-bisphosphonate-beta-blocker conjugate. C_{60} is an ideal scaffold for targeted drug delivery for the following reasons:

a. C_{60} is a biologically stable molecule that is non-toxic, non-immunogenic and efficiently cleared in mammals when it is properly derivatized.

b. C_{60} provides a versatile chemistry that allows external derivatization with medically-interesting materials such as drugs and biologically-active targeting

moieties such as peptides, antibodies, and in the present case, a beta-blocker drug.

The chemical structure of the targeted C_{60}-bisphosphonate-beta-blocker conjugate is shown in Figure 14. The carboxyl group of the tetralone of levobunolol has been reacted with a malonic hydrazide and then coupled to the C_{60}-Bis(bisphosphonate) compound of Chapter I via a Bingel reaction.

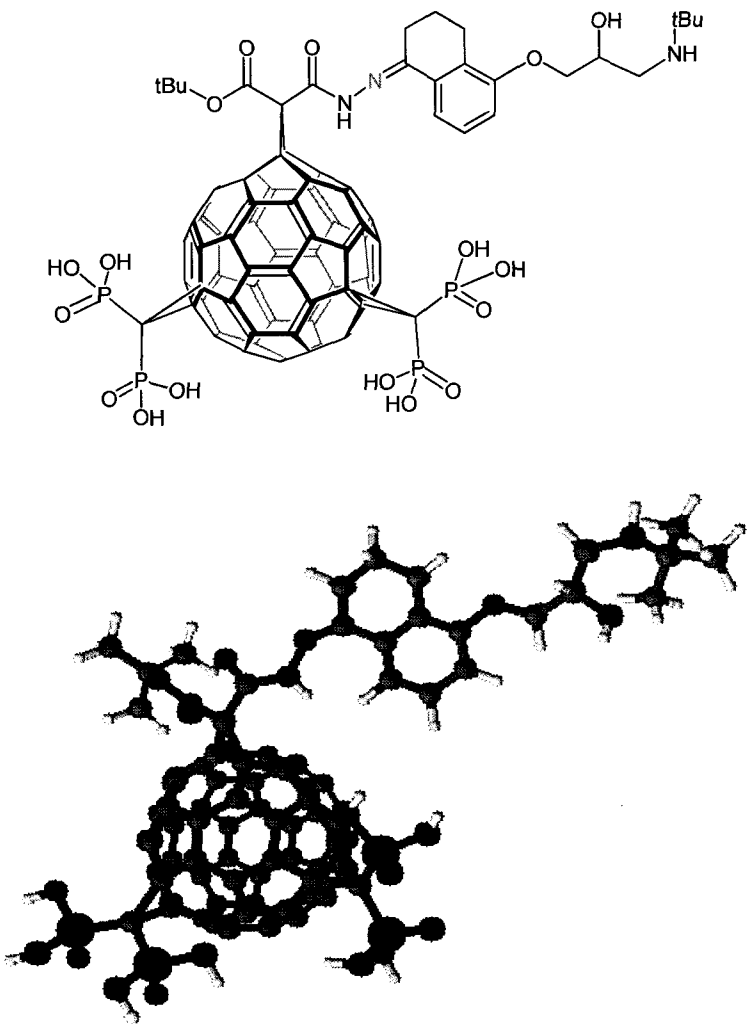

Figure 14. Three dimensional structure of the C_{60}-bisphosphonate-beta-blocker conjugate designed as a targeted treatment of osteoporosis; Top: 2-D view (hydrazone bond shown in blue); Bottom: 3-D view, gray = carbon, red = oxygen; blue = nitrogen; purple = phosphorous; white = hydrogen. Note that only one isomeric arrangement of the Bingel adducts is shown.

EXPERIMENTAL

Materials and Methods

All compounds were reagent grade or better. The following reagents were used as received: C_{60} (MER Corporation), anhydrous hydrazine (Aldrich), diethylmalonate (Aldrich), DBU (Aldrich), methyl-4-aminobutyrate HCl (Fluka), 5-methoxy-1-tetralone (Aldrich), tert-butyl-methyl malonate (Aldrich), triethylamine (Acros), DCC (Sigma), DIPEA (Alfa Aesar), levobunolol·HCl (BalPharma), sodium bicarbonate (Fisher), trimethylsilyl iodide (Aldrich) and di-tert-butyl dicarbonate (Fisher).

All solvents were of HPLC grade and purchased from Fisher. The following solvents were used as received: toluene, $CHCl_3$, acetone, H_2O, ethanol, methanol, 2-methoxy-ethanol, acetic acid, cyclohexane, anhydrous CCl_4, hexane and diethyl ether. CH_2Cl_2 was pre-dried with $CaCl_2$ and freshly distilled over P_2O_5.

All procedures for rendering anhydrous materials were carried under dry N_2 atmosphere. The N_2 (Trigas, prepurified) was purified by passing though a column containing R3-11 catalyst (Chemical Dynamics Corp.) on vermiculite to remove trace O_2 followed by trace H_2O removal with a column of Drierite ($CaSO_4$). For anhydrous reactions, all glassware was dried at 200 °C for at least 24 hours.

Flash chromatography was carried out using silica gel (70-230 mesh from EM science) after activation at 200 °C for at least 24 hours. TLC analyses were carried out using Whatman 250 μm layer silica gel with fluorescent indicator on polyester backing (PE SIL G/UV).

All ^{1}H and ^{13}C NMR spectra were recorded on a Bruker Avance 400 MHz spectrometer. All NMR solvents were from Cambridge Isotope Laboratories and were used as received.

Mass spectra were obtained on a Bruker MS Reflex IV MALDI-TOF mass spectrometer. For the MALDI-TOF spectra, unless otherwise specified, trans-2-[3-(4-tert-Butylphenyl)-2-methyl-2-propenylidene]malononitrile (DCTB) was used as matrix. The analytes were dissolved in an appropriate solvent and mixed with the matrix before spotting it on the sample plate.

Melting points were measured on a manual Melt-Temp® apparatus.

FT-IR spectra of the neat compounds were collected on a Nicolet Avatar FT-IR spectrometer, and the acquired data was processed using Origin® 7.5.

Syntheses

All new compounds for the synthesis of the C_{60}-bisphosphonate-beta-blocker conjugate have been fully characterized. The characterization data is at the end of the section for each compound and the spectral data can be found in the Appendix. Previously prepared compounds were fully characterized and compared to the literature data, and their selected spectra is presented in the Appendix.

Propanedioic acid, 1,3-dihydrazide (1). In a typical synthesis, 0.41 mL (12.68 mmol) of anhydrous hydrazine were added to a methanol/H_2O solution of 1.02 g (3.64 mmol) of diethylmalonate and stirred at room temperature for two hours. The resulting white solid was collected by filtration and dried. Yield 0.47g (97%); mp 153-4 °C. MALDI-TOF MS calcd. 132.1. Found 154.8 [M + Na^+].

Propanedioic acid, 1,3-bis[2-(1-methylethylidene)hydrazide] (2). A suspension of 0.20 g (1.51 mmol) of **1** in 3.5 mL of acetone was refluxed for two hours. The solid compound was collected by filtration and washed with 5 mL of ethanol and dried in vacuum. Yield 0.315 g (98%); mp 163–5 °C. MALDI-TOF MS calcd. 212.2. Found 286.4 [M + $NH_2Et_2^+$]. (matrix = α-Cyano-4-hydroxycinnamic acid diethylamine salt)

Propanedioic acid, 1,3-bis[2-(1-methylethylidene)hydrazide] C_{60} (3). C_{60} (500 mg, 0.694 mmol) was dissolved in 900 mL of toluene:CH_2Cl_2 (2:1). **2** (589 mg, 2.78 mmol) was dissolved in 20 mL of CH_2Cl_2 and added together with CBr_4 (921 mg, 2.78 mmol) to the C_{60} solution. DBU (158.24 mg, 2.78 mmol) in 30 mL of toluene was added to the solution over one hour. After stirring at room temperature for an additional two hours, the solvent was removed *in-vacuo*. The crude reaction mixture was chromatographed on silica gel using toluene as eluent to remove unreacted C_{60}. The mono, bis, tris and tetra adducts obtained were not separated. MALDI-TOF MS calcd. for adducts 930.92, 1141.16, 1351.39 and 1561.62. Found 931.42, 1141.51, 1351.61 and 1562.7 [M + H^+].

Methyl 4-[(3-tert-butoxy-3-oxopropanoyl)amino]butyrate (4). 5 g (42.68 mmol) of methyl 4-aminobutyrate hydrochloride, 6.41g (40.02 mmol) of mono-tert-Butyl malonate and 4.17 g (41.3 mmol) of triethylamine were dissolved in 1L of CH_2Cl_2 and cooled to 0°C. 10.99 g (53.3 mmol) of DCC were added and the mixture was stirred overnight letting the reaction reach room temperature. A few drops of acetic acid were added to precipitate all the N,N'-dicyclohexylurea and then the solution was filtered. The solvent was evaporated *in-vacuo* to leave an impure yellow oil. For further purification, 50 mL of

cyclohexane were added and left to rest for two hours in the refrigerator. The precipitate formed was filtered off, the solvent removed *in-vacuo* and the remaining oil was flash chromatographed on silica gel using CH_2Cl_2 as eluent. The solvent was removed again *in-vacuo* to give a clear oil as product. Yield 6.72 g (88 %). FT-IR (cm^{-1}) υ 3293 (s, N-H stretch), 2935 (m, C-H), 2862 (s, C-H), 1732 (s, ester C=O), 1651 (s, amide C=O), 1552 (s, N-H bend), 1437 (m, CH_2 bend), 1367 (s, CH_3 bend), 1253 (s, C−N stretch), 1145 (d, ester C−O). ^1H NMR ($CDCl_3$) δ 1.47 (s, 9H), 1.85 (p, 2H), 2.36 (t, 2H), 3.22 (s, 2H), 3.31 (q, 2H), 3.68 (s, 3H). MALDI-TOF MS calcd. 259. 29. Found 259.07 [M + H^+].

***Tert*-butyl 3-[(4-hydrazinyl-4-oxobutyl)amino]-3-oxopropanoate (5).** 2 g (7.71 mmol) of **4** were dissolved in 15 mL of methanol and 0.375 mL (11.95 mmol) of anhydrous hydrazine was added. The mixture was stirred at 50°C for two days while the progress of the reaction was monitored on ^1H-NMR. The solvent was evaporated *in-vacuo* giving a white solid. Yield: 1.98 g (99%). ^1H NMR ($CDCl_3$) δ 1.47 (s, 9H), 1.86 (p, 2H), 2.19 (t, 2H), 3.23 (s, 2H), 3.32 (q, 2H). MALDI-TOF MS calcd. 259. 29. Found 259.07 [M + H^+].

***Tert*-butyl 3-({4-[(2*Z*)-2-(5-methoxy-3,4-dihydronaphthalen-1(2*H*)-ylidene)hydrazinyl]-4-oxobutyl}amino)-3-oxopropanoate (6).** 728 mg (2.80 mmol) of **5** were dissolved in ethanol and 544 mg (3.09mmol) of 5-methoxy-1-tetralone were added. The mixture was allowed to stir for two days at 50 °C. The solvent was evaporated *in-vacuo* and the hydrazone was recrystallized from methanol as a white solid. Yield: 245 mg (21%). FT-IR (cm^{-1}) υ 3379 (s, N-H stretch), 2947 (m, C-H), 2867

(s, C-H), 1718 (s, ester C=O), 1662 (s, amide C=O), 1575 (s, C=N), 1523 (s, N-H bend), 1464 (m, CH_2 bend), 1346 (s, CH_3 bend), 1257 (s, C–N stretch), 1137 (d, ester C–O), 1037 (s, N-N). ^{1}H NMR ($CDCl_3$) δ 1.47 (s, 9H), 1.86 (p, 2H), 2.19 (t, 2H), 3.20 (s, 2H), 3.38 (q, 2H), 3.84 (s, 3H). ^{13}C NMR ($CDCl_3$) δ 21.97, 24.20, 27.01, 28.00, 30.26, 37.05, 39.20, 42.39, 55.54, 82.52, 101.94, 110.40, 116.58, 126.65, 128.88, 133.11, 147.16, 156.55, 165.57, 168.82, 175.12. MALDI-TOF MS calcd. 417.49. Found 417.03 [M + H^+].

***Tert*-butyl 3-({4-[(2*Z*)-2-(5-methoxy-3,4-dihydronaphthalen-1(2*H*)-ylidene)hydrazinyl]-4-oxobutyl}amino)-3-oxopropanoate C_{60} (7).** C_{60} (100 mg, 0.139 mmol) was dissolved in 100 mL of toluene:CH_2Cl_2 (2:1). Then **6** (58 mg, 0.139 mmol), CBr_4 (46.1 mg, 0.139 mmol), and DBU (21.2 mg, 0.139 mmol) were added. After stirring at room temperature for two hours, the reaction mixture was filtered and the solvent was removed *in-vacuo*. The crude reaction mixture was chromatographed on silica gel using CH_2Cl_2:methanol (20:1) to give mono and bis adducts. MALDI-TOF MS calcd. 1136.12 and 1551.64. Found 1136.84 and 1554.52 [M + H^+].

Protected levobunolol (8). A solution of di-tert-butyldicarbonate (100 mg, 0.46 mmol) in 3 mL of t-BuOH:H_2O (10:1) was added to a solution of levobunolol-HCl (150 mg, 0.46 mmol) and DIPEA (59.3 mg, 0.46 mmol) in 3 mL of t-BuOH:H_2O (10:1) and stirred for 24 hours at room temperature. Then the solution was poured onto 60 mL of water and extracted with hexane (3 x 30 mL). The combined organic layers were dried over Na_2SO_4. The mixture was filtered and the filtrate was concentrated *in-vacuo*. Further purification was performed by flash chromatography on silica gel using hexanes:diethyl

ether (1:1) as eluent to give the final product N-Boc-levobunolol as a white powder. Yield: 72 mg (35 %). FT-IR (cm^{-1}) υ 3359 (br, O-H stretch), 2976 (m, C-H), 2935 (s, C-H), 1740 (s, ester C=O), 1683 (s, amide C=O), 1471 (s, CH_2 bend), 1367 (s, CH_3 bend), 1262 (s, C–N stretch), 1162 (d, ester C–O). ^1H NMR ($CDCl_3$) δ 1.44 (s, 9H), 1.52 (s, 9H), 2.11 (ddddd, 2H), 2.63 (ddd, 2H), 2.89 (ddd, 2H), 2.96 (d, 2H), 3.73 (tt, 1H), 4.01 (d, 2H), 7.04 (dd, 1H), 7.27 (dd, 1H), 7.67 (dd, 1H). ^{13}C NMR ($CDCl_3$) δ 22.48, 22.89, 28.55, 29.94, 38.74, 48.85, 56.13, 70.43, 72.34, 81.22, 115.28, 119.21, 136.88, 133.67, 152.88, 155.68, 198.78. MALDI-TOF MS calcd. 391.50. Found 414.13 [M + Na^+].

***Tert*-butyl 3-hydrazinyl-3-oxopropanoate (9).** 2 g of tert-butyl methyl malonate were dissolved in methanol and 0.396 mL (12.63 mmol) of anhydrous hydrazine was added. The mixture was stirred at 50 °C, and after eight hours the solvent was removed *in-vacuo* to leave a white powder. Yield: 1.96 mg (98 %). FT-IR (cm^{-1}) υ 3300 (d, N-H stretch), 3201 (s, N-H stretch), 2979 (m, C-H), 2933 (s, C-H), 1728 (s, ester C=O), 1637 (s, amide C=O), 1525 (s, N-H bend), 1346 (s, CH_3 bend), 1307 (s, C–N stretch), 1147 (d, ester C–O), 1053 (s, N-N). ^1H NMR ($CDCl_3$) δ 1.47 (s, 3H), 3.26 (s, 2H). ^{13}C NMR ($CDCl_3$) δ 27.98, 41.13, 82.81, 166.34, 168.05. MALDI-TOF MS calcd. 174.19. Found 198.9 [M + Na^+].

Protected levobunolol malonate (10). To 72 mg (0.184 mmol) of **8** in 15 mL of 2-methoxy-ethanol 35 mg (0.202 mmol) of **9** were added. The solution was stirred overnight in an oil bath at 50 °C, the solvent was removed *in-vacuo* and the solid was purified by flash chromatography on silica gel using CH_2Cl_2:methanol (20:1) as eluent to

give a white powder as the final product. Yield 65.3 mg (64.8 %). FT-IR (cm^{-1}) υ 3398 (br, O-H stretch), 3197 (br, N-H stretch), 2974 (m, C-H), 2931 (s, C-H), 1734 (s, ester C=O), 1674 (s, amide C=O), 1575 (s, N-H bend), 1456 (s, CH_2 bend), 1365 (s, CH_3 bend), 1255 (s, C–N stretch), 1132 (d, ester C–O), 1037 (s, N-N). ^1H NMR ($CDCl_3$) δ 1.43 (s, 9H), 1.44 (s, 9H), 1.51 (s, 9H), 1.92 (ddddd, 2H), 2.59 (ddd, 2H), 2.74 (ddd, 2H), 3.62 (d, 2H), 3.70 (s, 2H), 3.71 (tt, 1H), 3.98 (d, 2H), 6.83 (dd, 1H), 7.16 (dd, 1H), 7.73 (dd, 1H). ^{13}C NMR ($CDCl_3$) 20.99, 21.97, 24.53, 28.00, 28.56, 29.92, 41.25, 42.81, 48.89, 56.07, 70.28, 72.33, 80.97, 81.56, 111.27, 117.37, 126.48, 128.80, 133.13, 147.95, 155.42, 158.53, 166.86, 169.65. MALDI-TOF MS calcd. 547.68. Found 573.12 [M + Na^+].

Protected levobunolol malonate C_{60} (11). C_{60} (86 mg, 0.119 mmol) was dissolved in 100 mL of toluene: CH_2Cl_2 (2:1), and then **10** (65.3mg, 0.119 mmol), CBr_4 (39.5 mg, 0.119 mmol), and DBU (18 mg, 0.119 mmol) were added. After stirring at room temperature for two hours, the reaction mixture was filtered and the solvent was removed *in-vacuo*. The crude reaction mixture was chromatographed on silica gel using CH_2Cl_2:methanol (20:1) as eluent to give a mono-adduct. MALDI-TOF MS calcd. 1266.30. Found 1265.52 [M + H^+].

C_{60}-Bisphosphonate-Beta-Blocker Conjugate (12). $C_{60}[C(PO_3iPr_2)_2]_2$ (50 mg, 0.0357 mmol) was dissolved in 100 mL of toluene: CH_2Cl_2 (2:1), and then **10** (19.5 mg, 0.036 mmol), CBr_4 (11.8 mg, 0.036 mmol), and DBU (5.5 mg, 0.036 mmol) were added. After stirring at room temperature for two hours, the reaction mixture was filtered and the

solvent was removed *in-vacuo*. The crude reaction mixture was chromatographed on silica gel using EtOAC as eluent. After removal of unreacted $C_{60}[C(PO_3iPr_2)_2]_2$, the C_{60}-bisphosphonate-beta-blocker conjugate was collected. MALDI-TOF MS calcd. 1950.91. Found 1950.37 $[M + H^+]$.

Hydrolysis and Deprotection of C_{60}-Bisphosphonate-Beta-Blocker Conjugate (13). 19.5 mg (0.01 mmol) of **12** were treated with a 1.5 excess of trimethylsilyl iodide (24 mg, 0.12 mmol) in dry CCl_4 at 45 °C for one hour and left stirring overnight. Transformation to the diphosphonic acid was achieved by treating with excess of 1% $NaHCO_3$ aqueous solution for one hour for the pH to remain neutral. Later, the aqueous layer was extracted and rotoevaporated. The resulting compound was dialyzed to get rid of excess salts. The water was removes *in-vacuo* and the sample lyophilized.

RESULTS AND DISCUSSION

Synthesis and Characterization of the C_{60}-Bisphosphonate-Beta-Blocker Conjugate

The strategy for the C_{60}-bisphosphonate-beta-blocker conjugate synthesis involved the synthesis of a malonohydrazide derivative and coupling it to levobunolol via a hydrazone bond, followed by the attachment to C_{60}. Since hydrazide compounds have not been previously coupled to C_{60}, two model compounds were first prepared. This synthetic sequence was designed to minimize the number of steps involving levobunolol due to its high cost.

The first synthesis involved the preparation of malonodihydrazide **1** according to Jung et. al and its reaction with acetone to form hydrazone **2**.[62] The Bingel reaction of **2**

with C_{60} with *in-situ* generation of the brominated intermediate gave compound **3**. The Bingel reaction (nucleophilic cyclopropanation) was used since it was by far the simplest and most versatile method of C_{60} derivatization. This reaction, like most fullerene derivatization procedures, afforded a mixture of mono, bis, tris a tetraaducts.

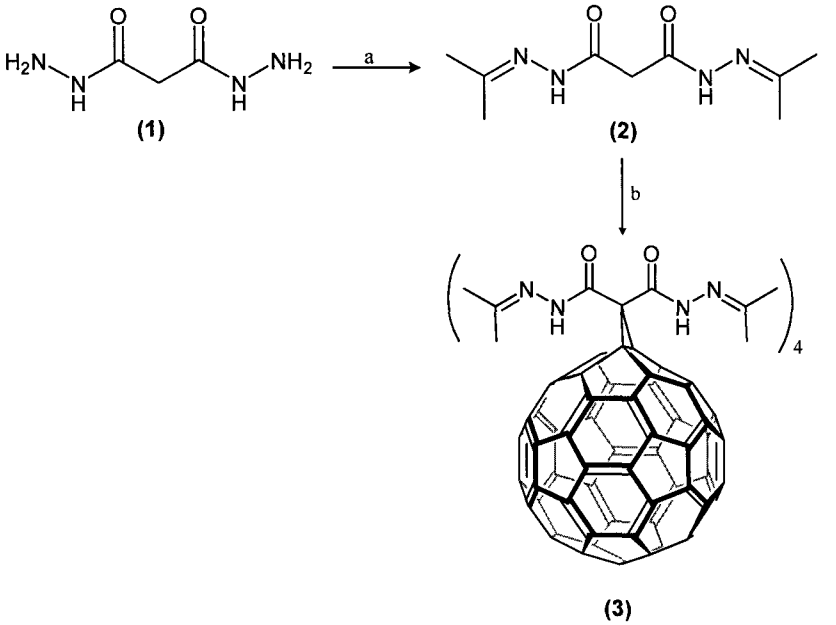

Figure 15. Synthesis of the first C_{60}-hydrazone model compound (**3**). (a) acetone (b) C_{60}, CBr_4, DBU, toluene:CH_2Cl_2 (2:1).

Once it was established that a hydrazone could be coupled to C_{60} via a Bingel reaction, a second model compound reaction was designed. For this reaction, the ketone chosen had a tetralone group similar to the levobunolol molecule. Malonate **4** was formed by reacting mono-tert-butyl malonate and methyl-4-aminobutyrate HCl in the presence of DCC. After addition of dry hydrazine, hydrazide **5** was formed. 5-methoxy-1-tetralone was then coupled to **5** forming hydrazone **6**. This hydrazone malonate was coupled to C_{60} via a Bingel reaction forming C_{60}-hydrazone compound **7**.

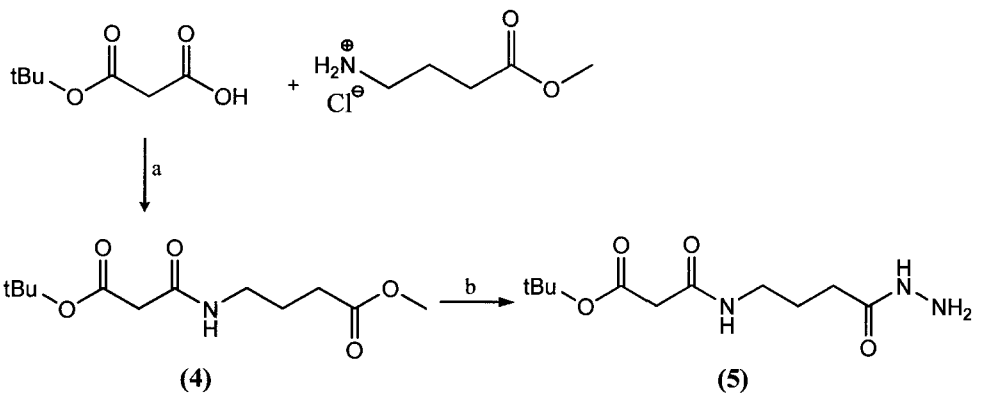

Figure 16. Synthesis of *tert*-butyl 3-[(4-hydrazinyl-4-oxobutyl)amino]-3-oxopropanoate (**5**). (a) Et_3N, DCC, CH_2Cl_2, 88%; (b) anhydrous N_2H_4, methanol, 99%.

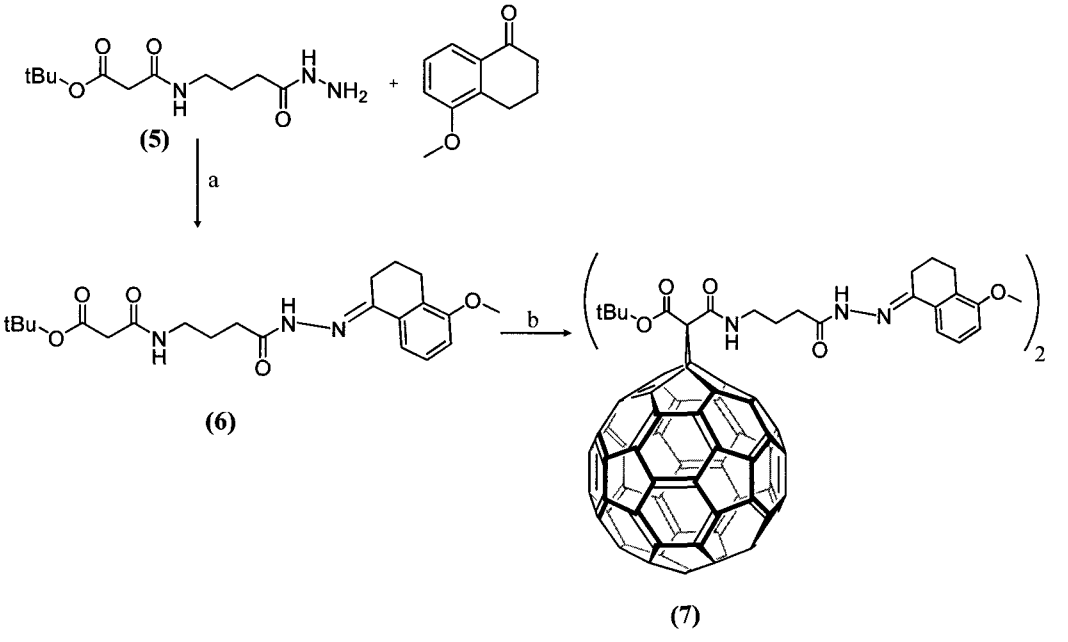

Figure 17. Synthesis of the second C_{60}-hydrazone model compound (**7**). (a) ethanol, 21%; (b) C_{60}, CBr_4, DBU, toluene;CH_2Cl_2(2:1).

The long arm provided by the aminobutyrate was first thought to provide better stability upon reaction with C_{60} and to prevent levobunolol·HCl from reacting with C_{60}. However, the amide formation reaction was too slow and the side product, N,N'-dicyclohexylurea, kept precipitating. Therefore, it was decided that just a simple reaction of **9** with protected levobunolol **8** to form the hydrazone **10**, and the subsequent Bingel

reaction with C_{60} would finally afford the desired C_{60}-beta-blocker conjugate **11** (Figure 19).

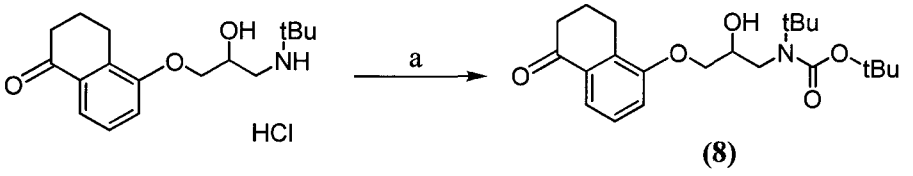

Figure 18. Protection of levobunolol (**8**).(a) Boc_2O, DIPEA, t-BuOH:H_20 (10:1).

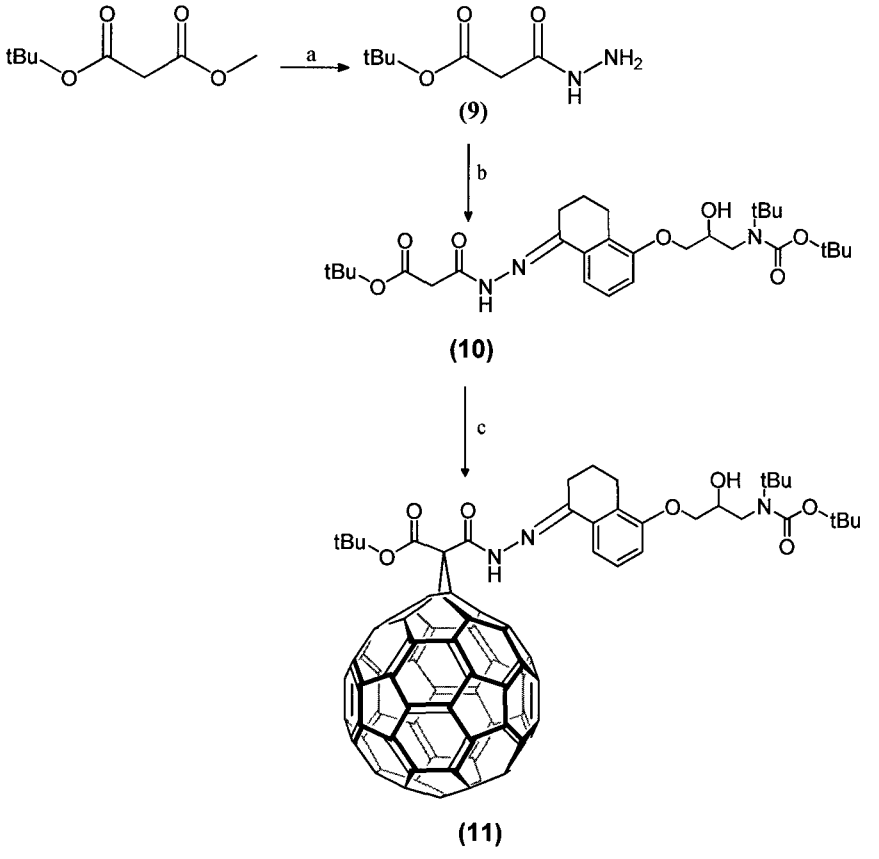

Figure 19. Synthesis of the C_{60}-beta-blocker conjugate (**11**). (a) anhydrous N_2H_4, methanol, (b) protected levobunolol, 2-methoxy-ethanol, (c) CBr_4, DBU, toluene;CH_2Cl_2(2:1).

The formation of the **11** gave rise to the first C_{60}-beta-blocker derivative needed to finally form the sought-after C_{60}-bisphosphonate-beta-blocker conjugate. Thus, when **10** was reacted with $C_{60}[C(PO_3iPr_2)_2]_2$ in the presence of DBU and CBr_4, the protected

C_{60}-bisphosphonate-beta-blocker conjugate **12** was finally obtained, while its water soluble form **13** was ultimately obtained by deprotection with $Si(CH_3)_3I$ (Figure 20).

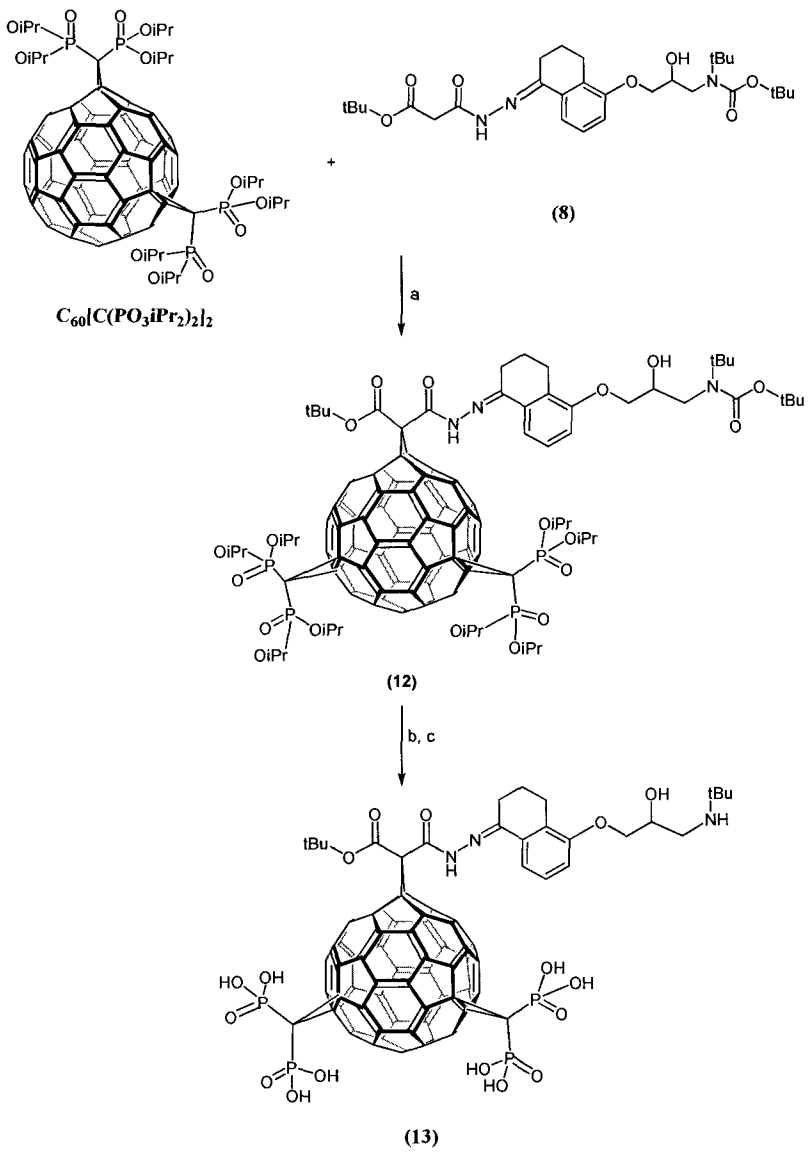

Figure 20. Synthesis of the C_{60}-Bisphosphonate-Beta-blocker Conjugate (**13**). (a) CBr_4, DBU, toluene;CH_2Cl_2(2:1), (b) $Si(CH_3)_3I$, CCl_4, (c) 1% $NaHCO_3$(aq). Only one possible geometrical isomer of **12** is shown.

MALDI-TOF MS data for the C_{60}-bisphosphonate-beta-blocker conjugate are consistent with the assigned structure. The presence of the conjugate was verified by MALDI-TOF MS with the molecular ion peak at *m/z* =1949 (Figure 20).

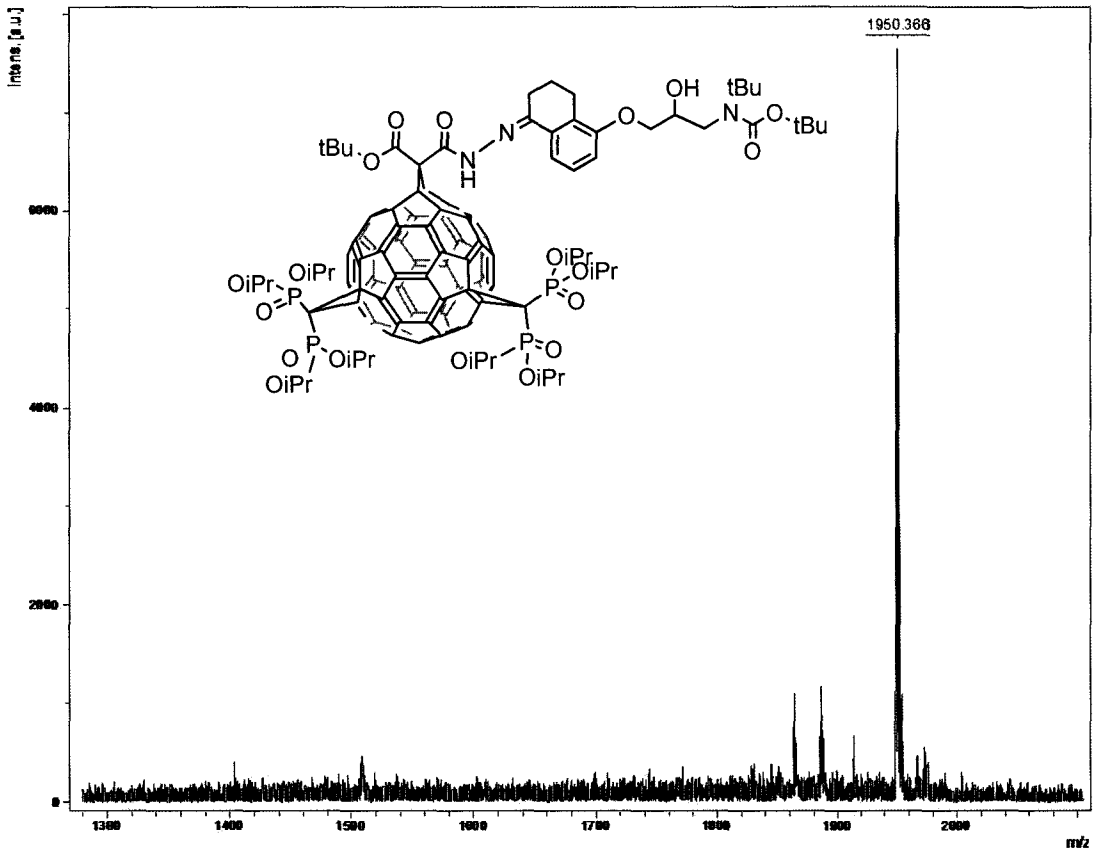

Figure 21. MALDI-TOF MS mass spectrum of **12**.

NMR Analysis

Even though the ^{13}C NMR of C_{60} fullerene is simple, attachment of functional groups to C_{60} results in a decrease of symmetry for the molecule. The single resonance of C_{60} is split into many small peaks, thus complicating the spectra of reaction products. To resolve the numerous peaks in the fullerene region, long acquisition times are required. However, if multiple geometrical isomeric C_{60}-derivatives are formed, as it is the case of the C_{60}-Bisphophonate-Beta-blocker Conjugate, assigning the carbon peaks becomes nearly impossible.

The ^{1}H NMR spectra of C_{60} fullerene multi-adducts generally give very complex patterns, mainly due to the presence of multiple isomers and the tendency of C_{60} to trap

solvent molecules in the lattice, which also causes solvent proton signals to appear in the spectrum. The ^{1}H NMR spectrum of compound **12** was taken, and although it is expectedly complex, regions belonging to the expected proton signals were identified as shown in Figure 22. In addition, the corresponding ^{13}C NMR spectrum was taken and can be seen in Figure 23.

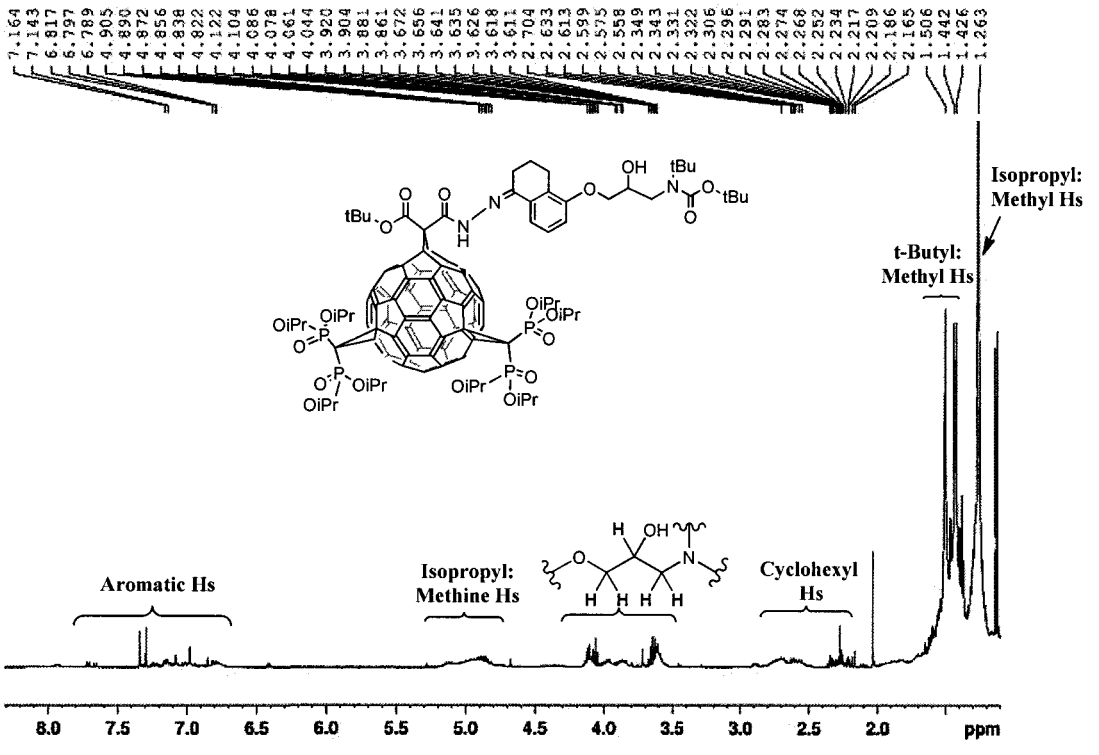

Figure 22. ^{1}H NMR spectrum of **12** in $CDCl_3$.

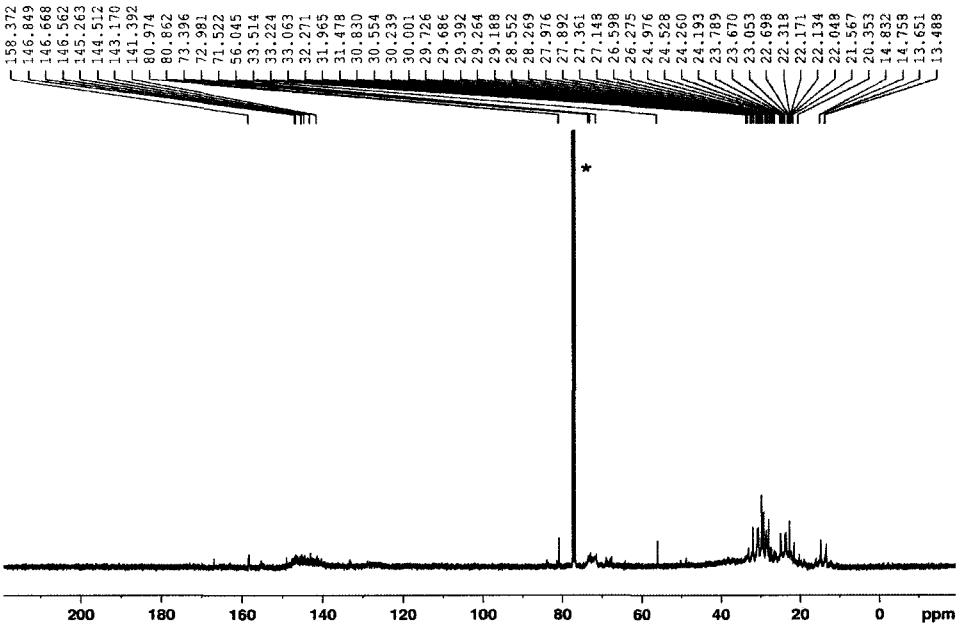

Figure 23. ^{13}C NMR spectrum of **12** in $CDCl_3$. (* = solvent peak).

CONCLUSIONS

In this work, the synthesis and complete characterization of the first C_{60}-bisphosphonate-beta-blocker conjugate has been performed as a targeted therapy for osteoporosis. Levobunolol was derivatized by forming a hydrazone bond with a hydrazide malonate and later coupled to C_{60} via Bingle chemistry to form compound **11**. This beta-blocker hydrazone malonate was then added to the C_{60}-bisphosphonate compound from Chapter I to yield the desired C_{60}-bisphosphonate-beta-blocker conjugate **13** which is water soluble. Pharmacokinetics and osteoblast inhibition studies of compound **13** in animal models are under investigation in Dr. Gerard Karsenty's laboratories at Columbia University.

APPENDIX

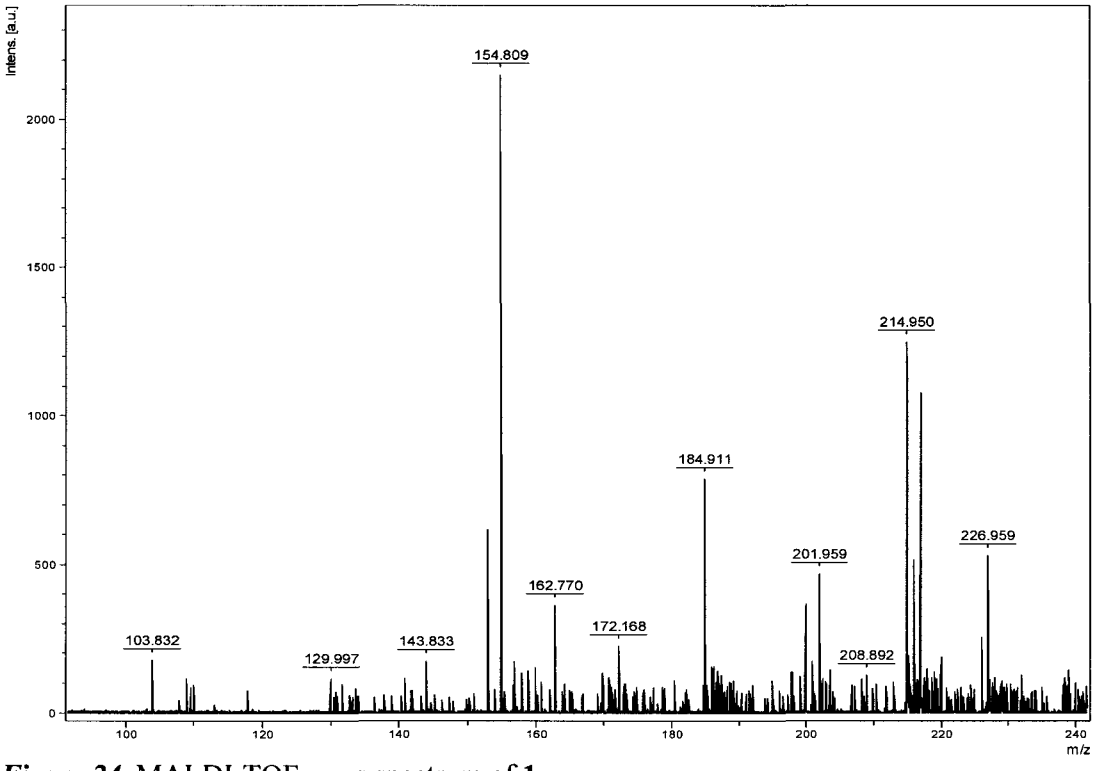

Figure 24. MALDI-TOF mass spectrum of **1.**

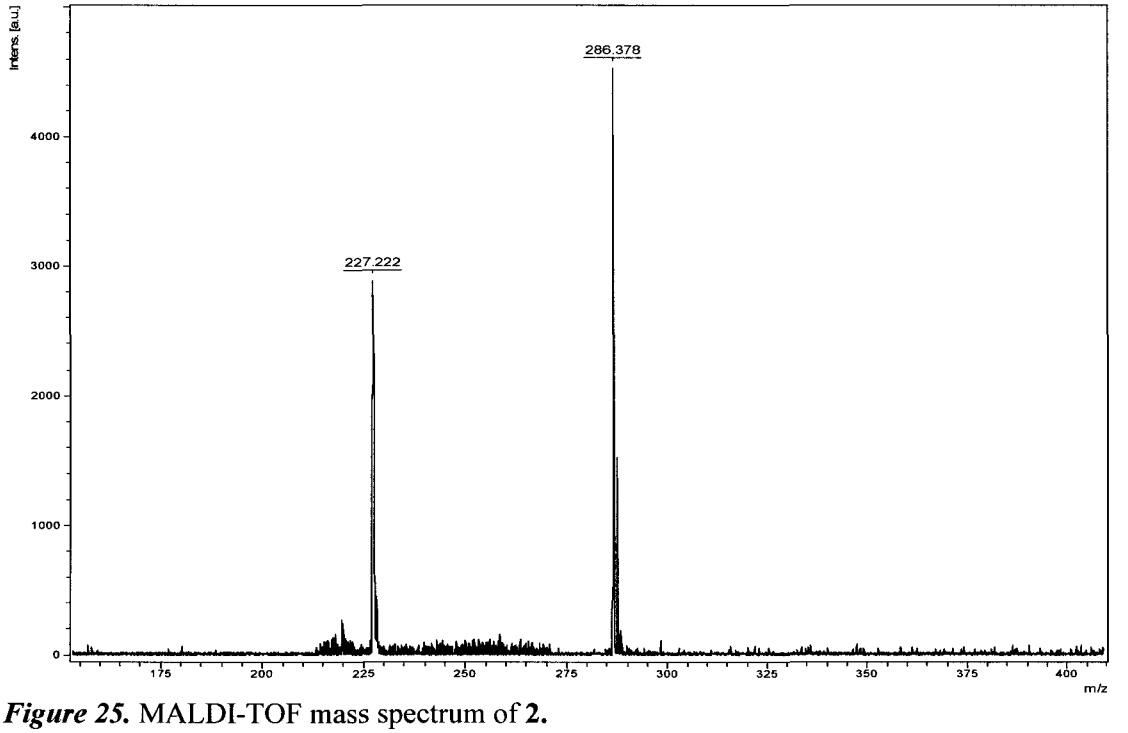

Figure 25. MALDI-TOF mass spectrum of **2.**

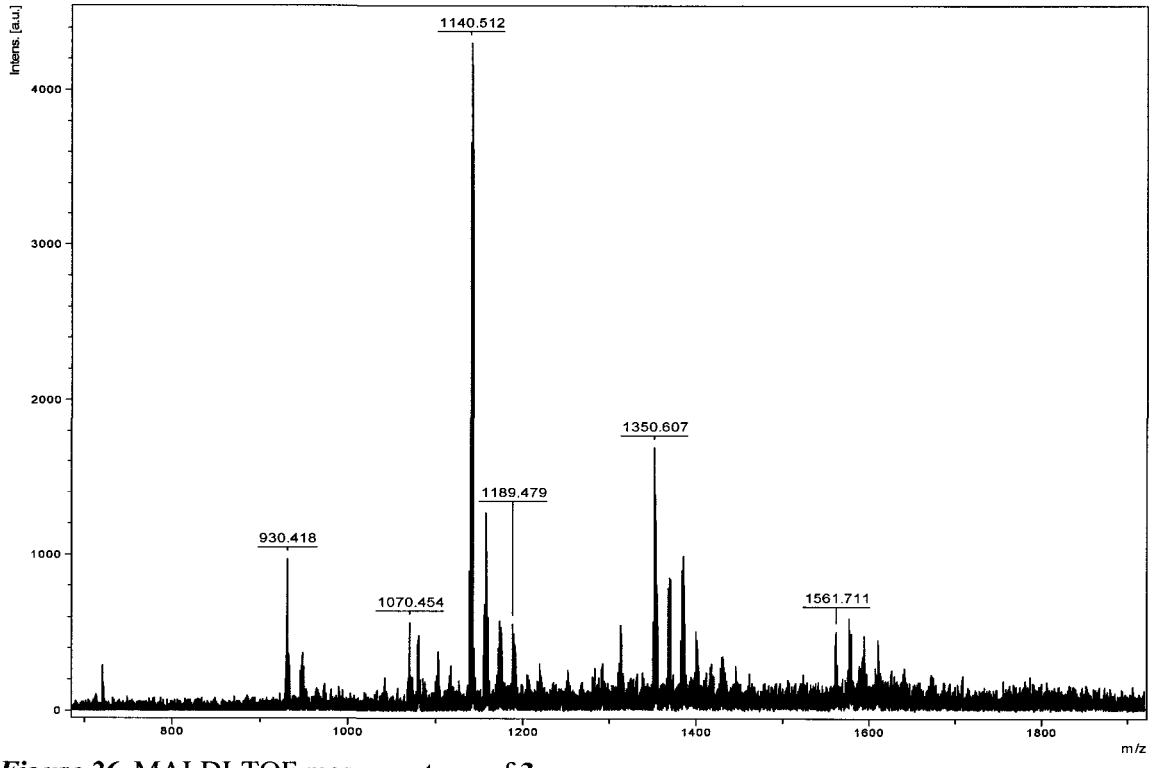

Figure 26. MALDI-TOF mass spectrum of **3.**

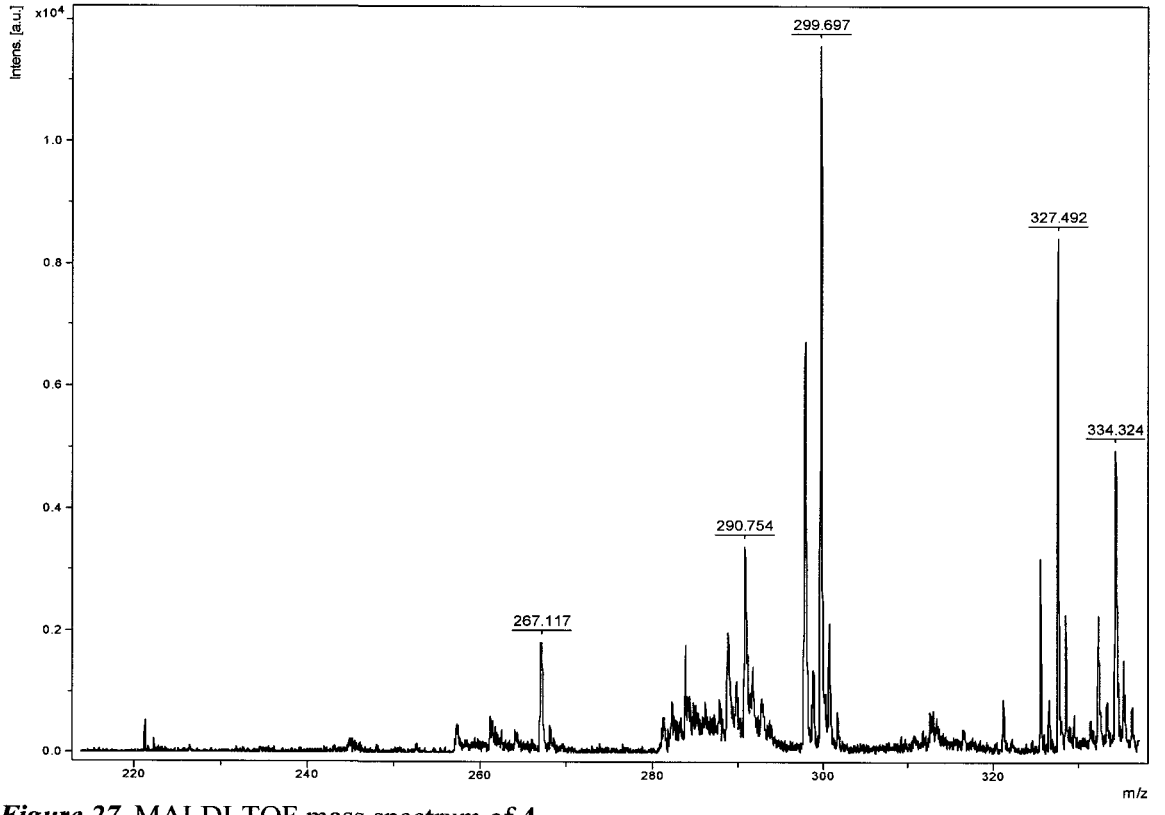

Figure 27. MALDI-TOF mass spectrum of **4.**

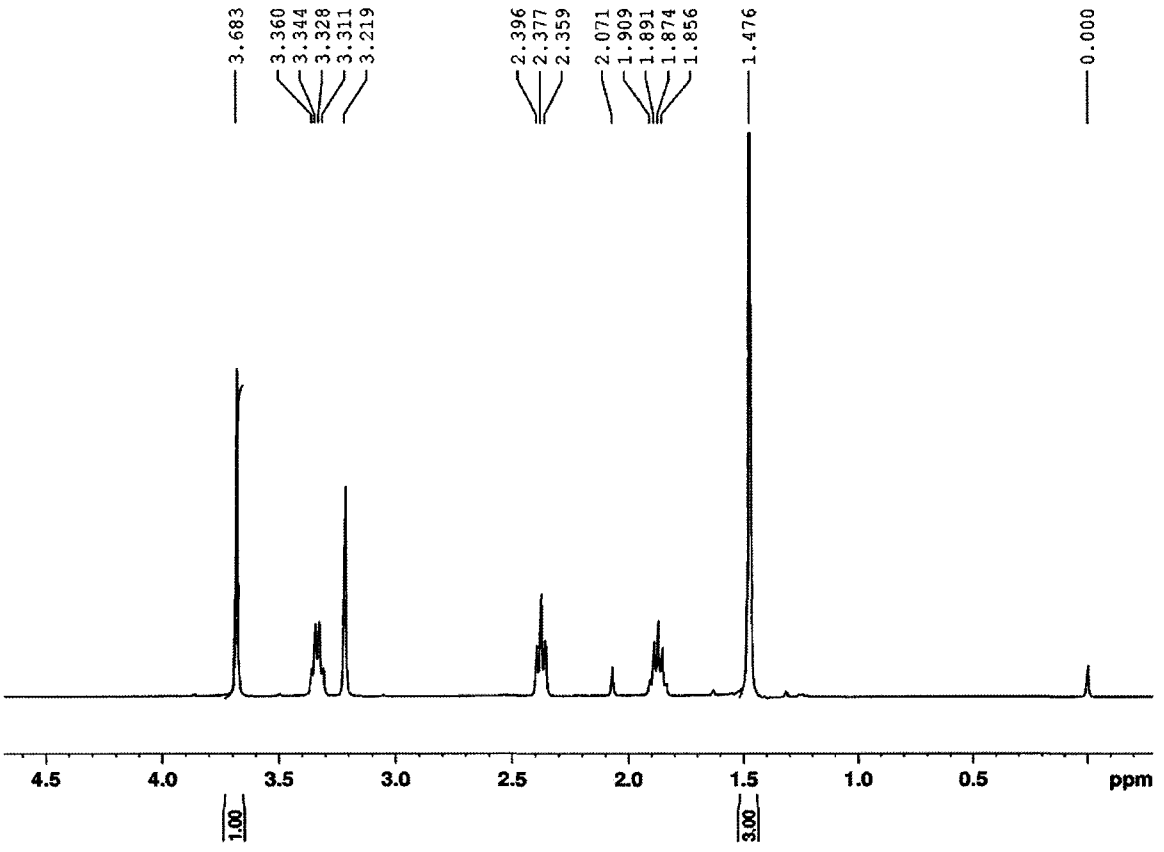

Figure 28. ^{1}H NMR spectrum of **4** in $CDCl_3$.

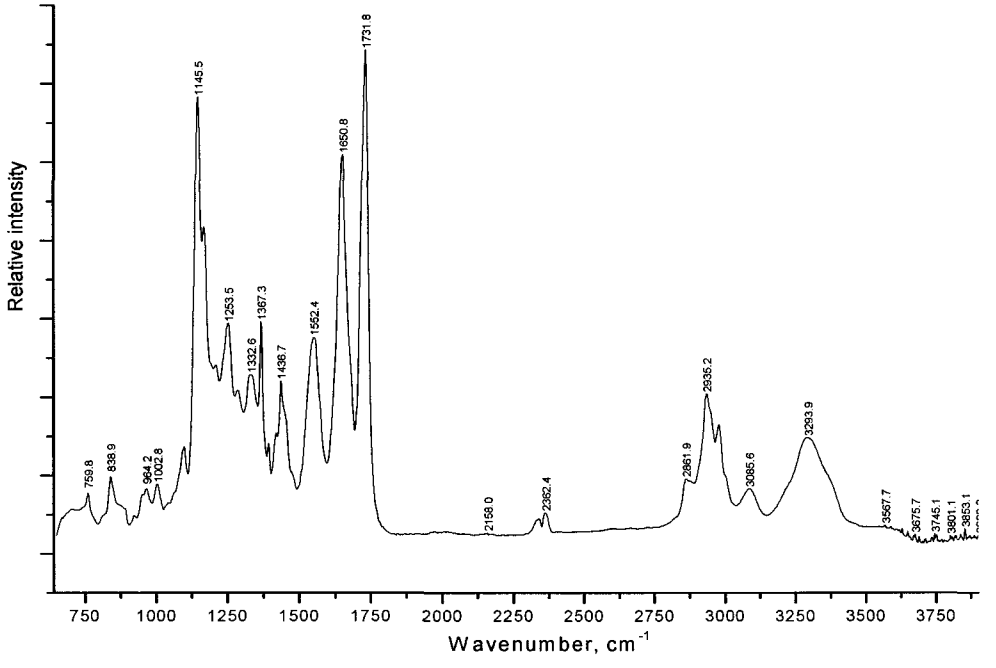

Figure 29. FT-IR spectrum of **4.**

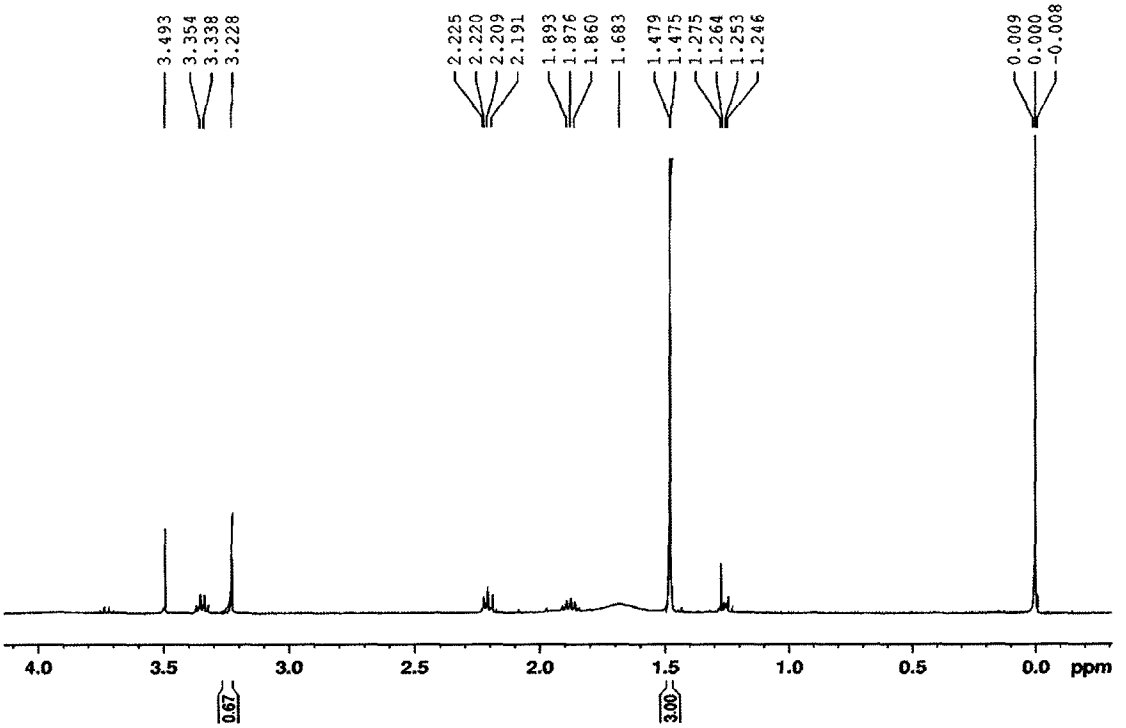

Figure 30. ^{1}H NMR spectrum of **5** in $CDCl_3$.

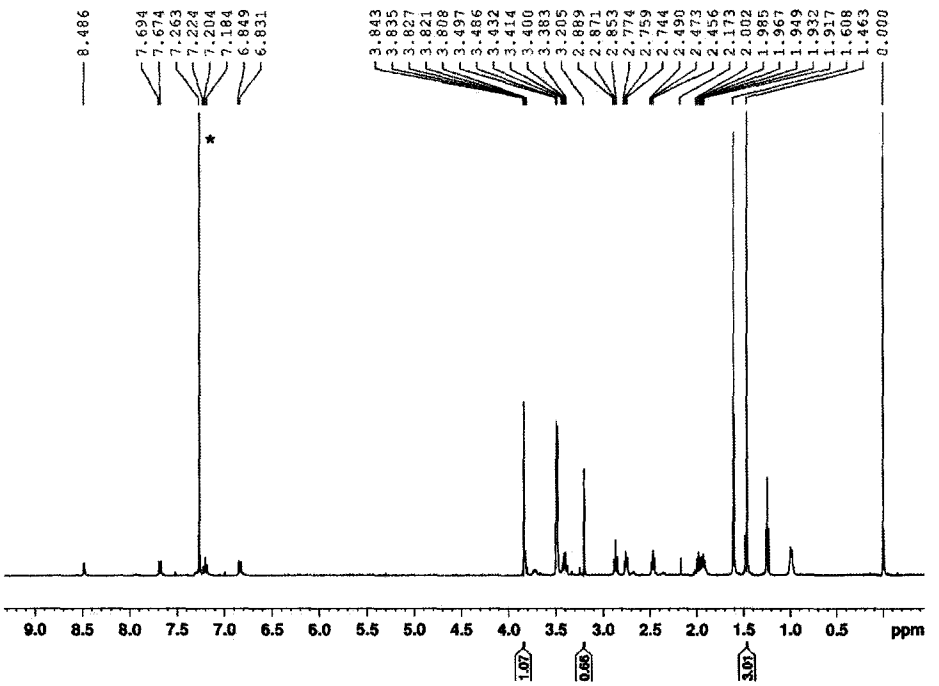

Figure 31. ^{1}H NMR spectrum of **6** in $CDCl_3$. (* = solvent peak)

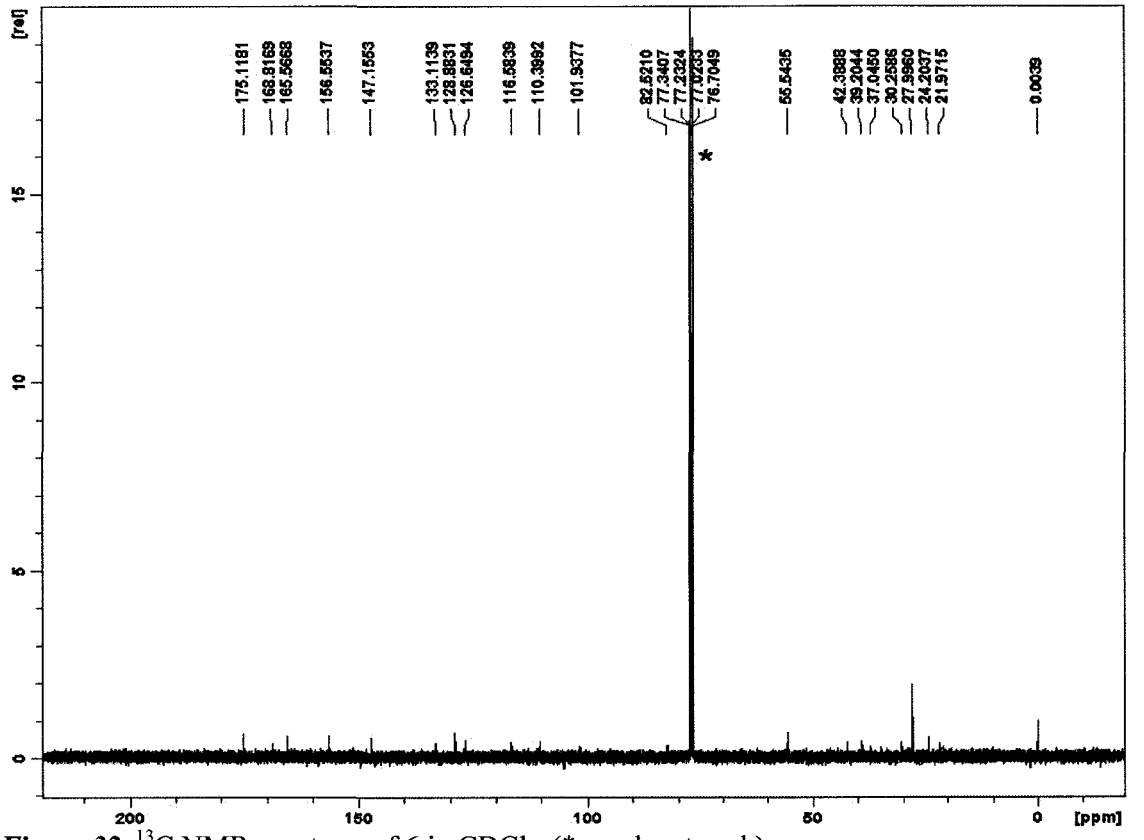

Figure 32. ^{13}C NMR spectrum of **6** in $CDCl_3$. (* = solvent peak)

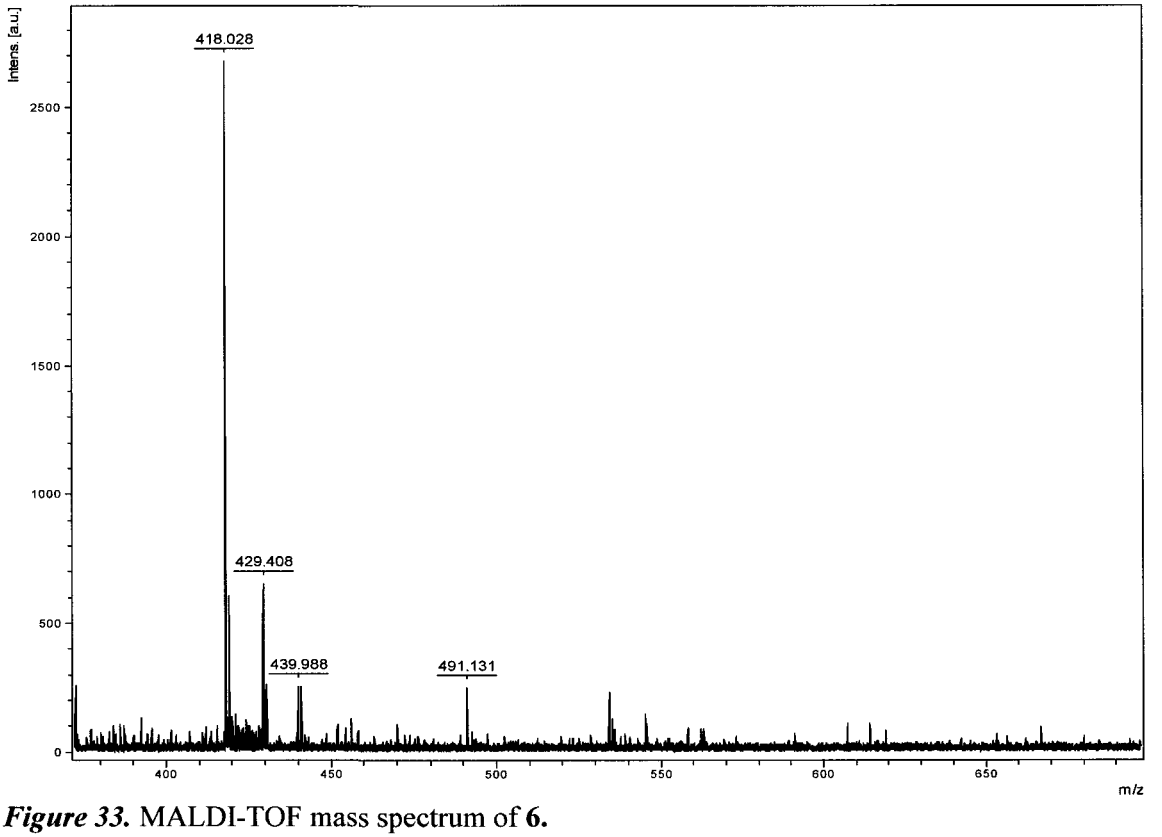

Figure 33. MALDI-TOF mass spectrum of **6.**

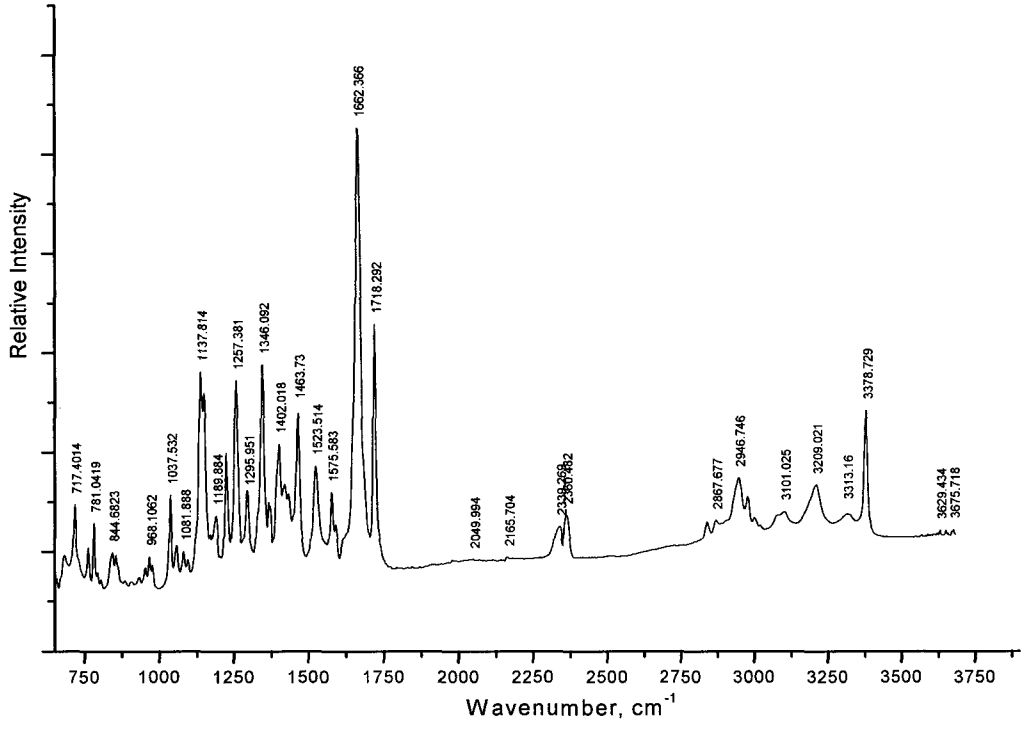

Figure 34. FT-IR spectrum of **6.**

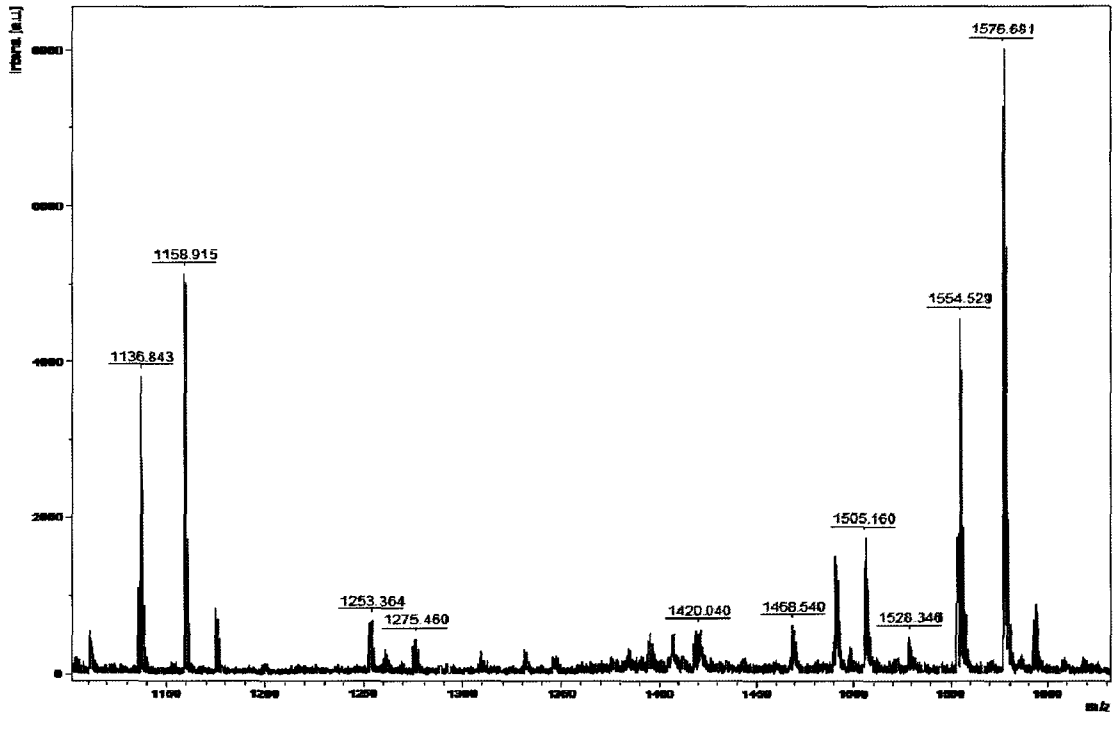

Figure 35. MALDI-TOF mass spectrum of **7.**

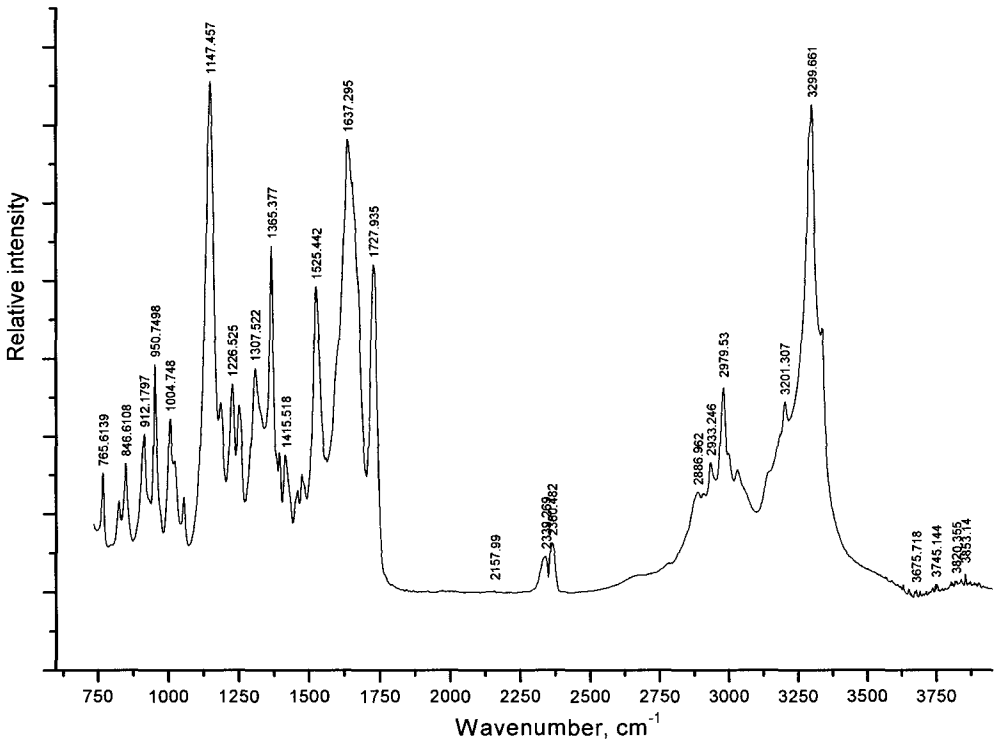

Figure 36. FT-IR spectrum of **9.**

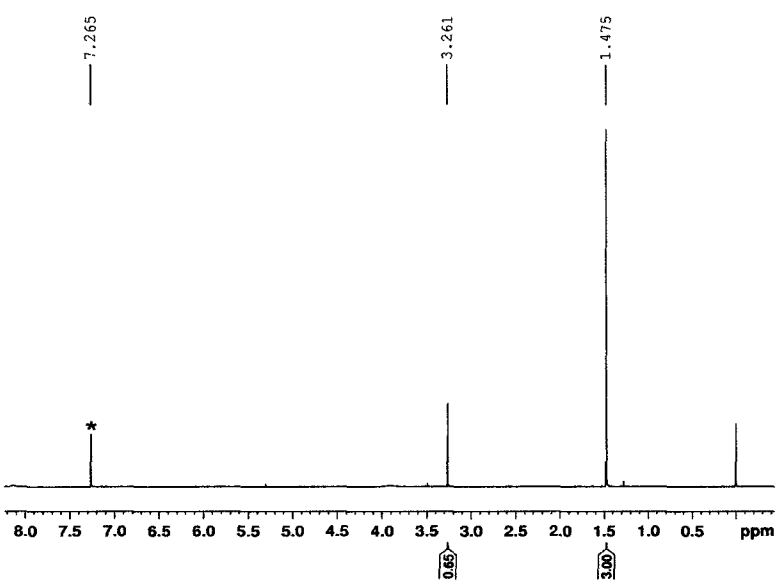

Figure 37. ^{1}H NMR spectrum of **9** in $CDCl_3$. (* = solvent peak)

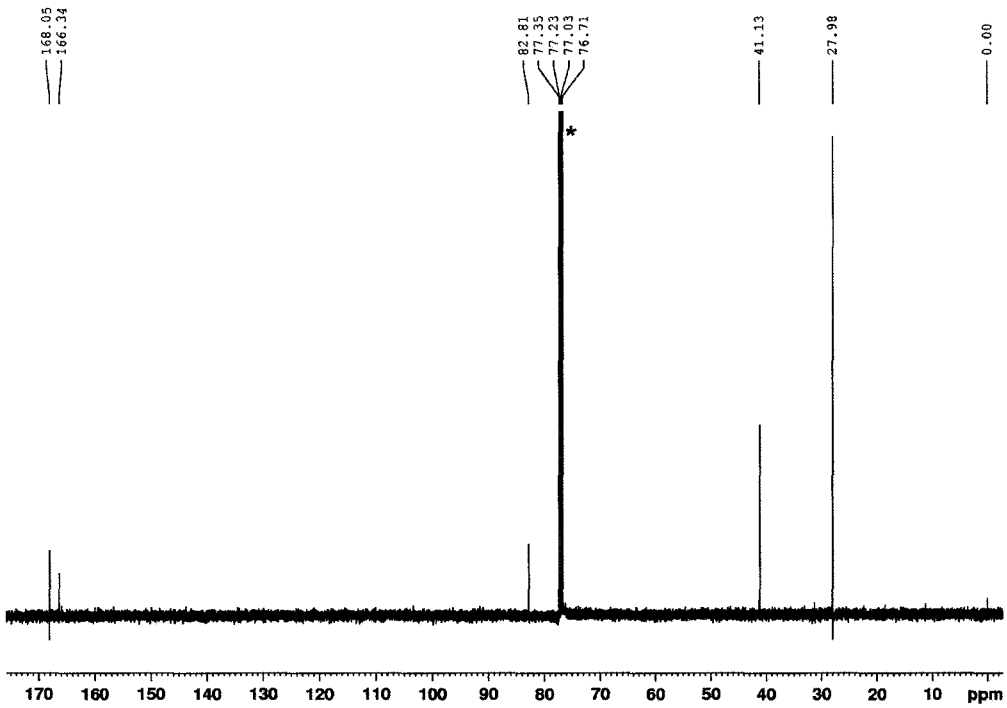

Figure 38. ^{13}C NMR spectrum of **9** in $CDCl_3$. (* = solvent peak)

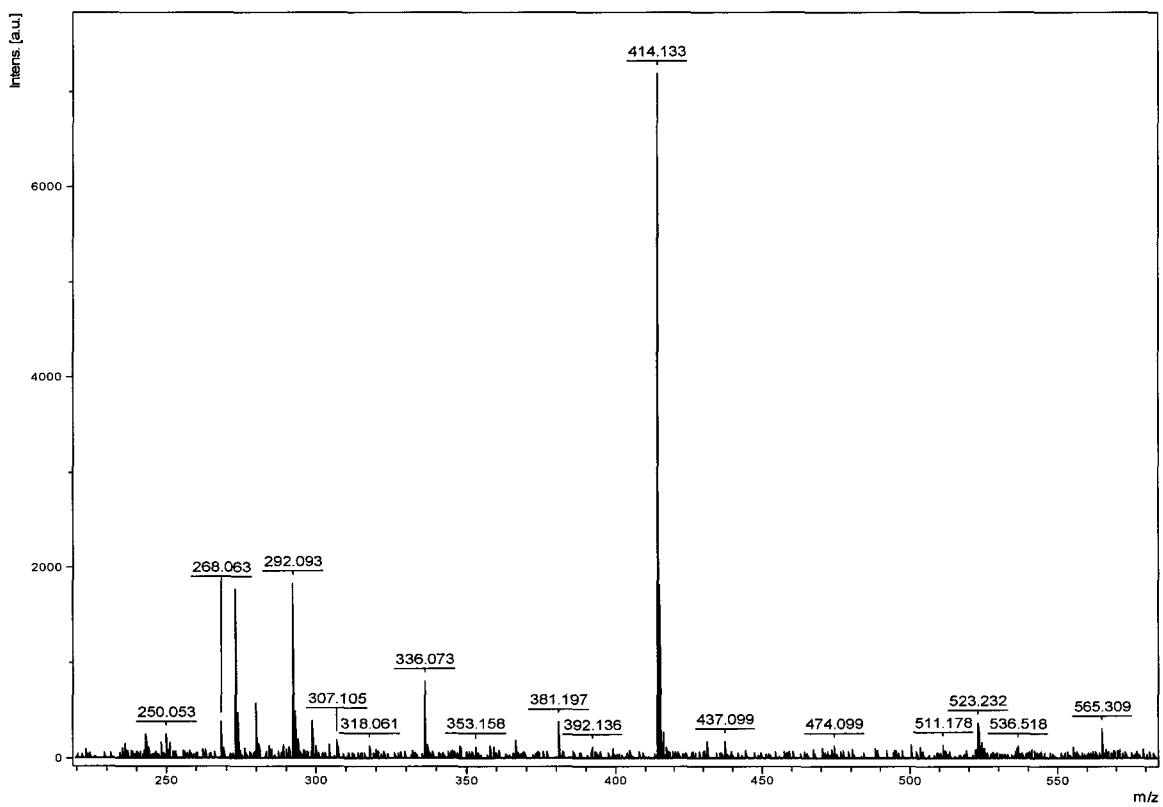

Figure 39. MALDI-TOF mass spectrum of **8.**

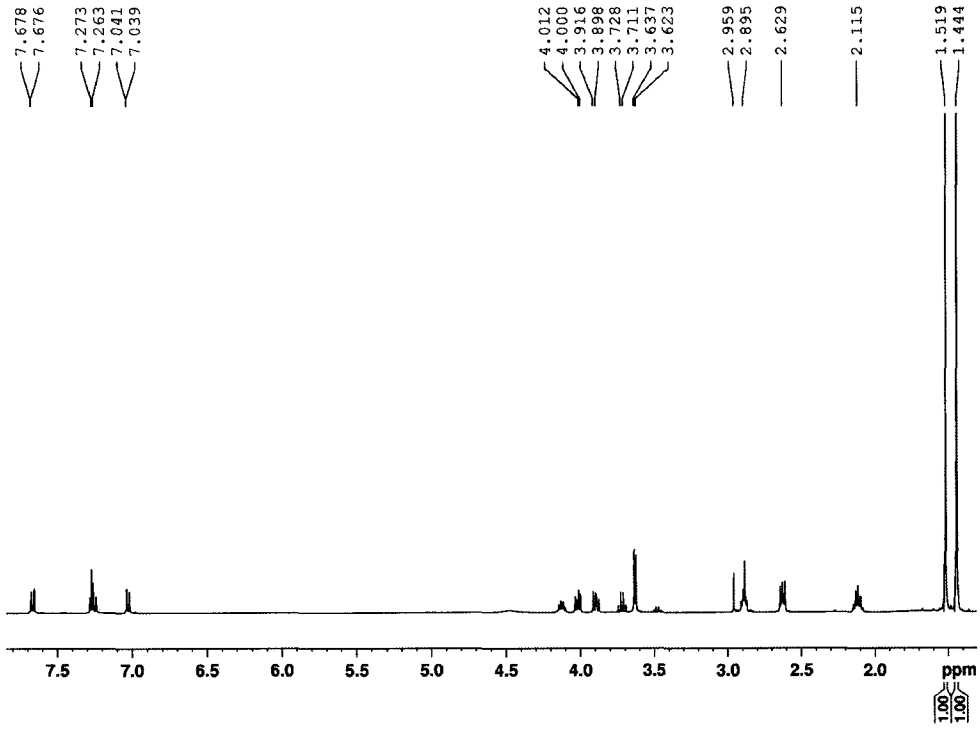

Figure 40. ^{1}H NMR spectrum of **8** in $CDCl_3$.

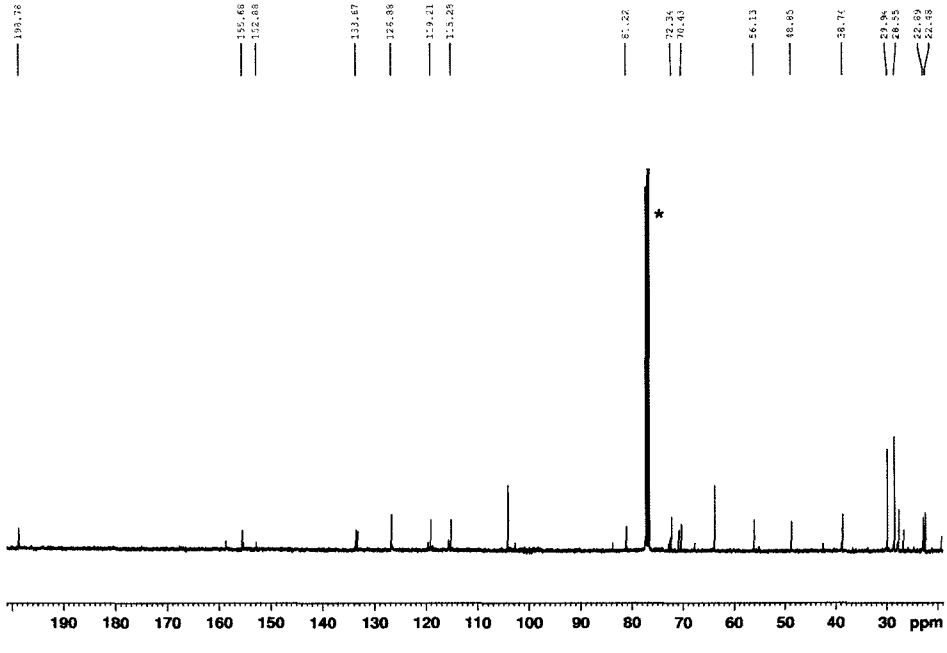

Figure 41. ^{13}C NMR spectrum of **8** in $CDCl_3$. (* = solvent peak)

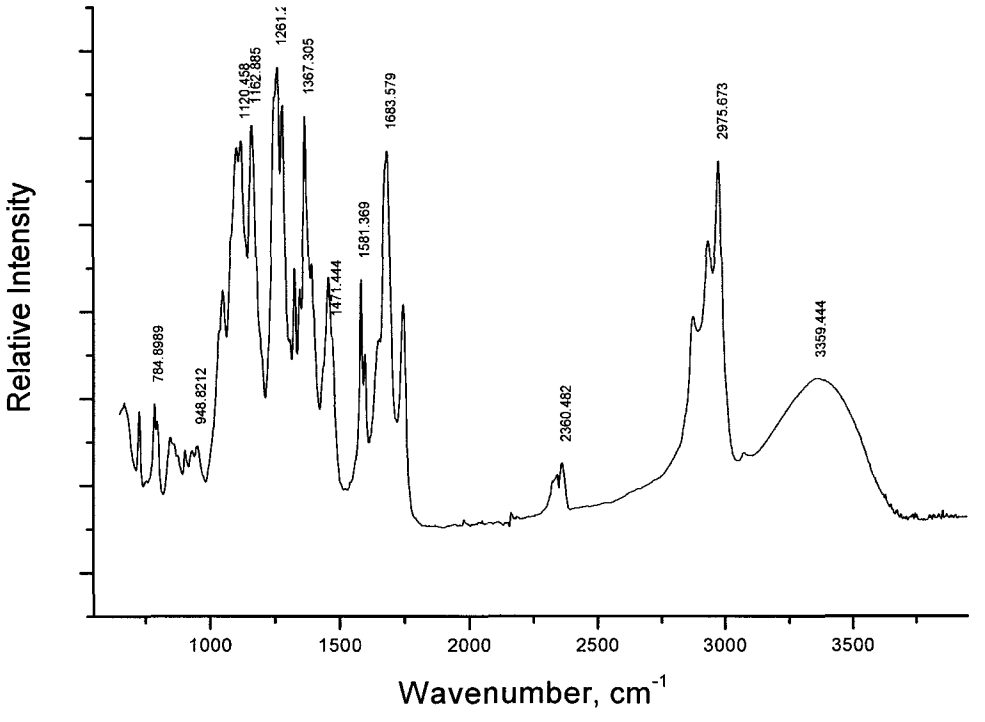

Figure 42. FT-IR spectrum of **8.**

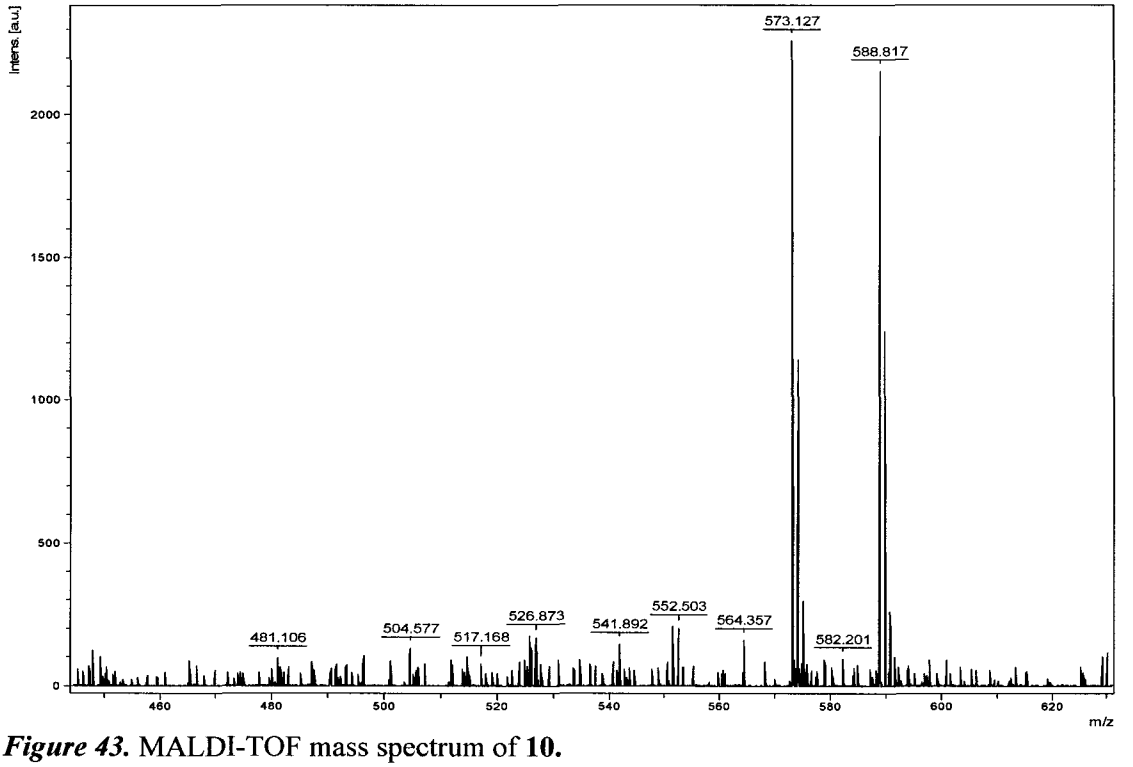

Figure 43. MALDI-TOF mass spectrum of **10.**

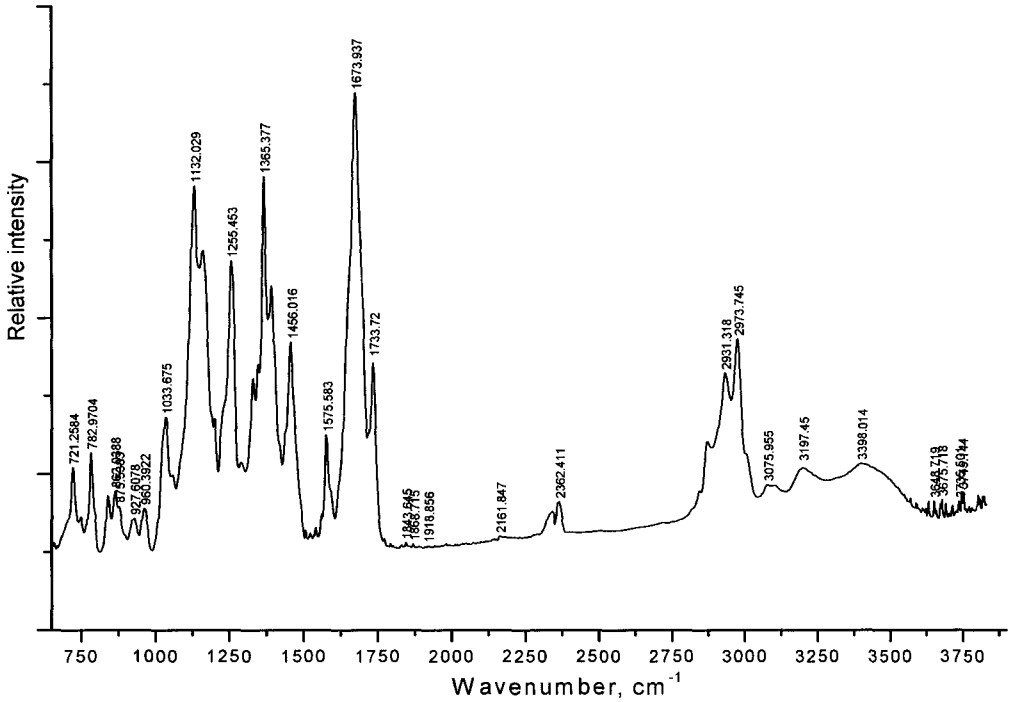

Figure 44. FT-IR spectrum of **10.**

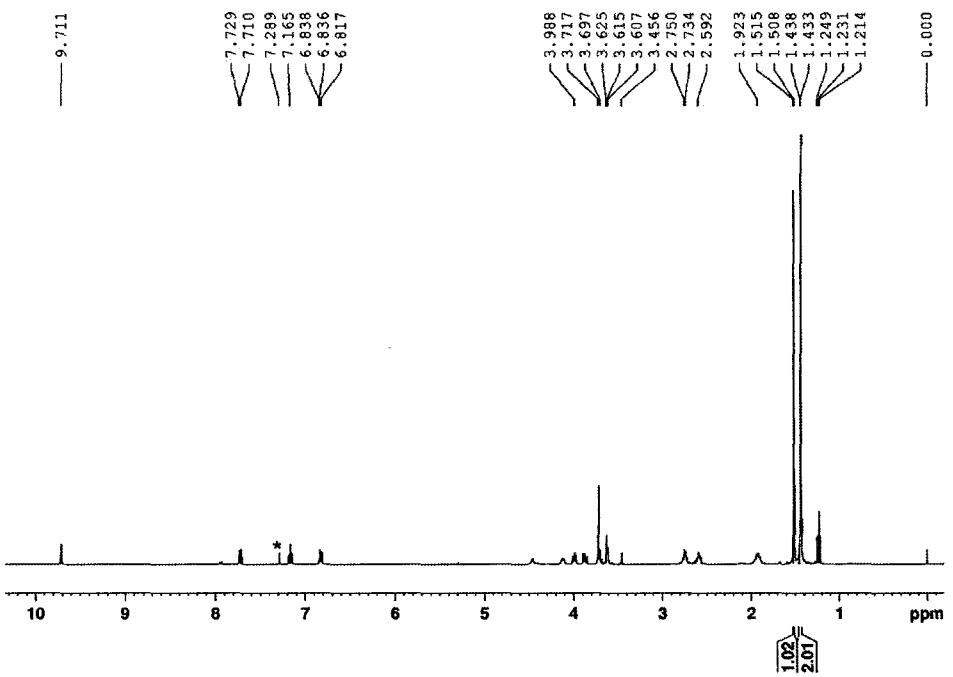

Figure 45. ^{1}H NMR spectrum of **10** in $CDCl_3$. (* = solvent peak)

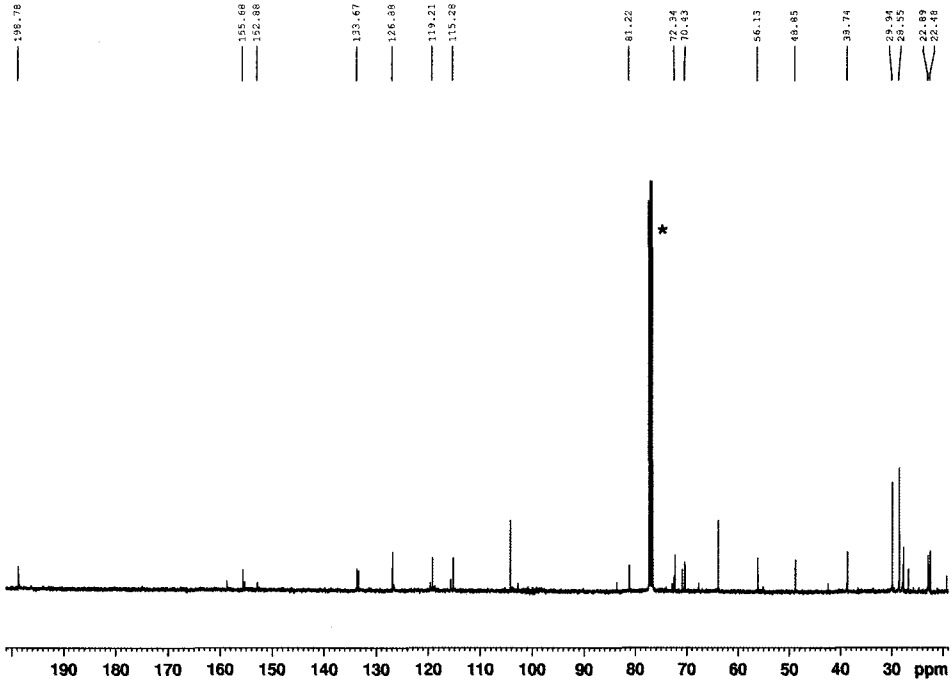

Figure 46. ^{13}C NMR spectrum of **10** in $CDCl_3$. (* = solvent peak)

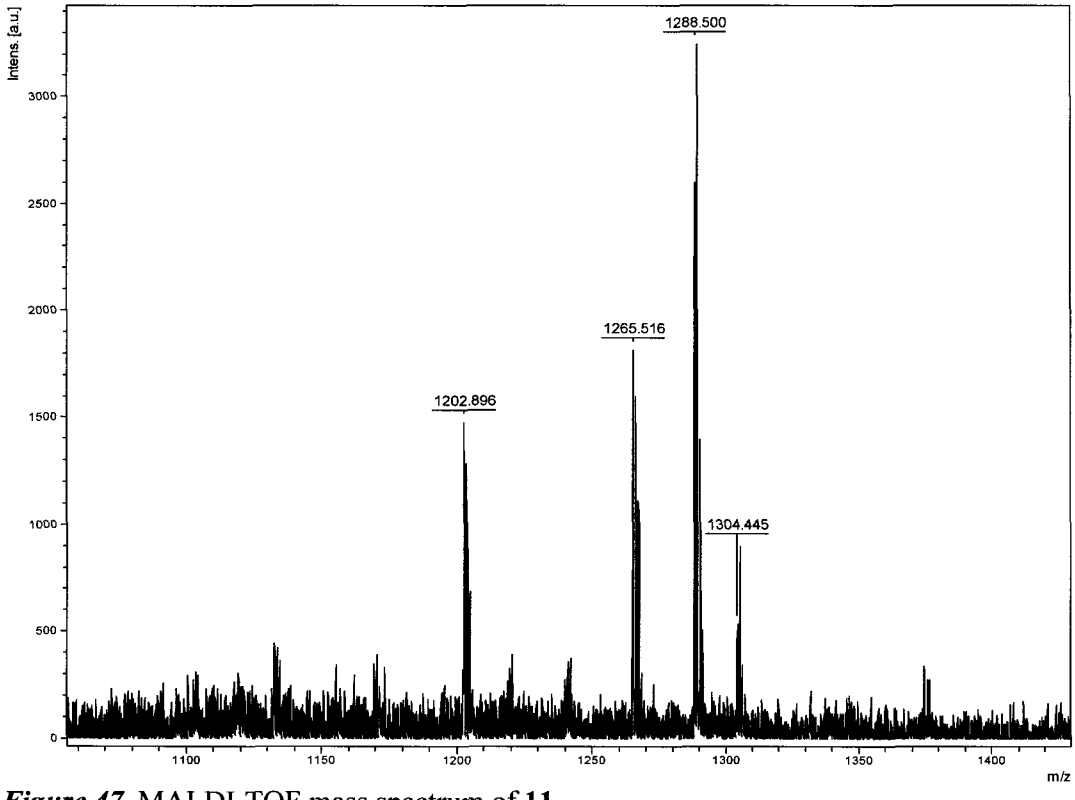

Figure 47. MALDI-TOF mass spectrum of **11.**

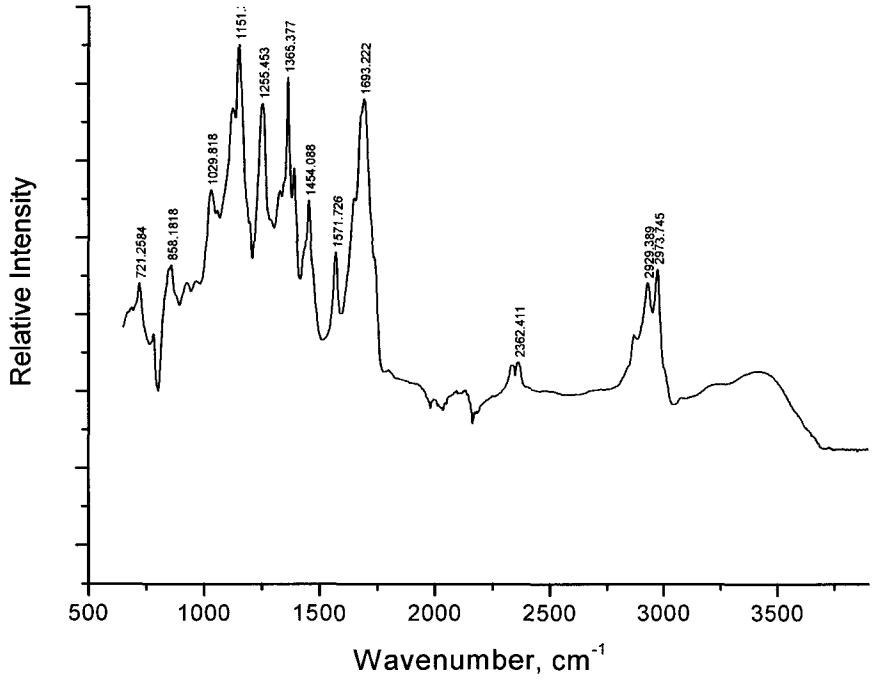

Figure 48. FT-IR spectrum of **11.**

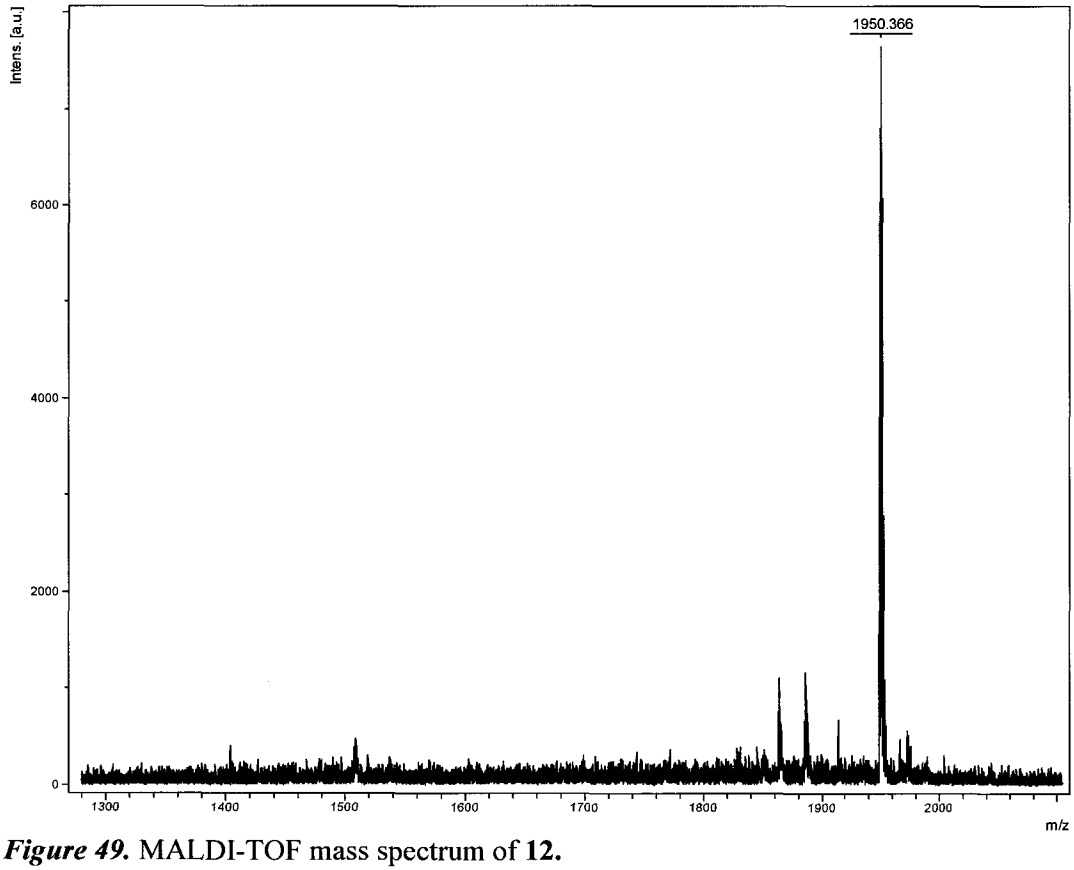

Figure 49. MALDI-TOF mass spectrum of **12.**

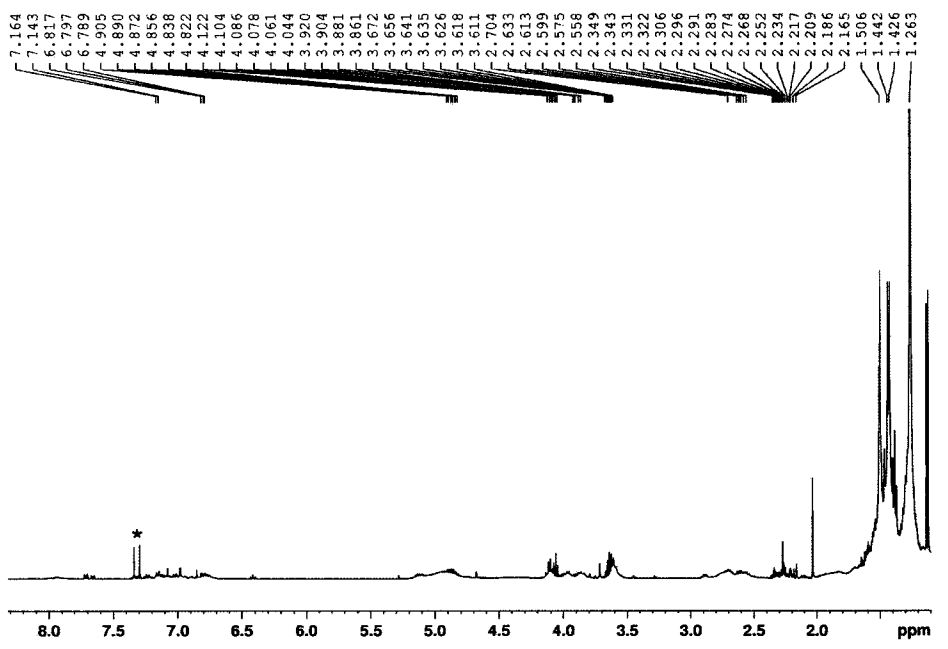

Figure 50. ^{1}H NMR spectrum of **12** in $CDCl_3$. (* = solvent peak)

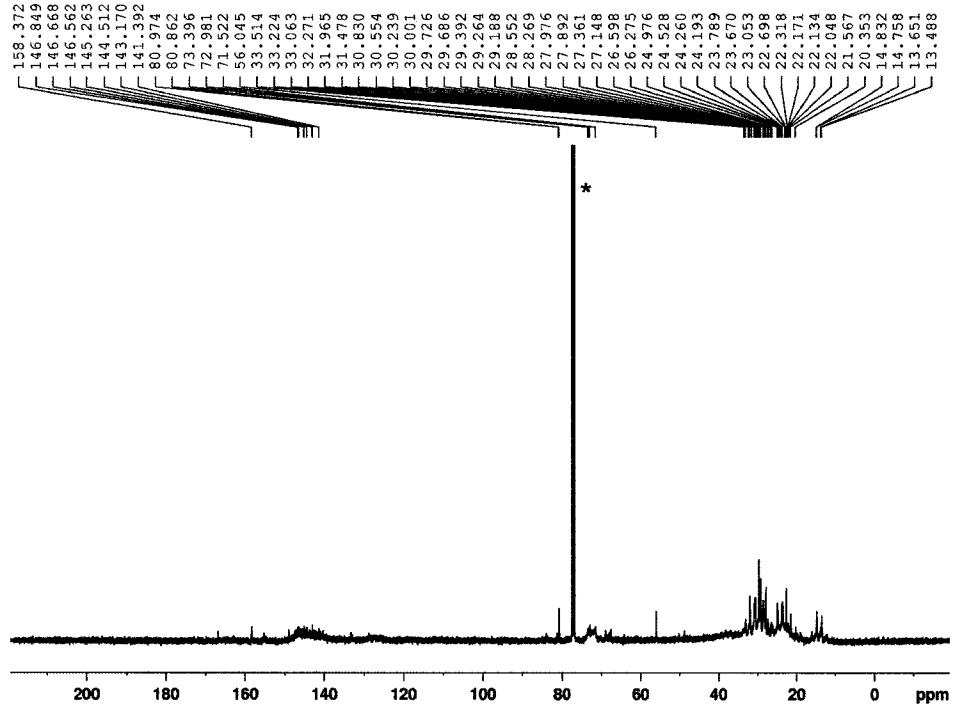

Figure 51. ^{13}C NMR spectrum of **12** in $CDCl_3$. (* = solvent peak)

REFERENCES

1. Kaiser, M.; Reichenbach, J.; Byrne, H. J.; Anders, J.; Maser, W.; Roth, S., *Synth. Met.* **1992,** *51* (1-3), 251-6.
2. Kelty, S. P.; Chen, C. C.; Lieber, C. M., *Nature (London)* **1991,** *352* (6332), 223-5.
3. Lee, C. H.; Yu, G.; Moses, D.; Srdanov, V. I.; Wei, X.; Vardeny, Z. V., *Phys. Rev. B: Condens. Matter* **1993,** (11), 8506-9.
4. Minami, N., *Mol. Cryst. Liq. Cryst. Sci. Technol., Sect. A* **1992,** *217*, 231-4.
5. Yonehara, H.; Pac, C., *Appl. Phys. Lett.* **1992,** *61* (5), 575-6.
6. Hungerbuehler, H.; Guldi, D. M.; Asmus, K. D., *Journal of the American Chemical Society* **1993,** *115* (8), 3386-7.
7. Yamakoshi, Y. N.; Yagami, T.; Fukuhara, K.; Sueyoshi, S.; Miyata, N., *J. Chem. Soc., Chem. Commun.* **1994,** (4), 517-18.
8. Oberdorster, G.; Sharp, Z.; Atudorei, V.; Elder, A.; Gelein, R.; Kreyling, W.; Cox, C., *Inhal. Toxicol.* **2004,** *16* (6-7), 437-45.
9. Dugan, L. L.; Turetsky, D. M.; Du, C.; Lobner, D.; Wheeler, M.; Almli, C. R.; Shen, C. K.; Luh, T. Y.; Choi, D. W.; Lin, T. S., *Proc Natl Acad Sci* **1997,** *94* (17), 9434-9.
10. Friedman, S. H.; DeCamp, D. L.; Sijbesma, R. P.; Srdanov, G.; Wudl, F.; Kenyon, G. L., *J. Am. Chem. Soc.* **1993,** *115* (15), 6506-9.
11. Tokuyama, H.; Yamago, S.; Nakamura, E.; Shiraki, T.; Sugiura, Y., *J. Am. Chem. Soc.* **1993,** *115* (17), 7918-19.

12. Bolskar, R. D.; Benedetto, A. F.; Husebo, L. O.; Price, R. E.; Jackson, E. F.; Wallace, S.; Wilson, L. J.; Alford, J. M., *J. Am. Chem. Soc.* **2003,** *125* (18), 5471-5478.

13. Cagle, D. W.; Kennel, S. J.; Mirzadeh, S.; Alford, J. M.; Wilson, L. J., *Proc. Natl. Acad. Sci.* **1999,** *96* (9), 5182-5187.

14. Zakharian, T. Y.; Seryshev, A.; Sitharaman, B.; Gilbert, B. E.; Knight, V.; Wilson, L. J., *J. Am. Chem. Soc.* **2005,** *127* (36), 12508-12509.

15. Ashcroft, J. M.; Tsyboulski, D. A.; Hartman, K. B.; Zakharian, T. Y.; Marks, J. W.; Weisman, R. B.; Rosenblum, M. G.; Wilson, L. J., *Chem. Commun.* **2006,** (28), 3004-3006.

16. Sitharaman, B.; Zakharian, T. Y.; Saraf, A.; Misra, P.; Ashcroft, J.; Pan, S.; Pham, Q. P.; Mikos, A. G.; Wilson, L. J.; Engler, D. A., *Mol. Pharmaceutics* **2008,** *5* (4), 567-578.

17. Gonzalez, K. A.; Wilson, L. J.; Wu, W.; Nancollas, G. H., *Bioorg. Med. Chem.* **2002,** *10* (6), 1991-1997.

18. Mirakyan, A. L.; Wilson, L. J., *J. Chem. Soc., Perkin Trans. 2* **2002,** (6), 1173-1176.

19. Reynolds, I. J.; Hastings, T. G., *J. Neurosci.* **1995,** *15* (5, Pt. 1), 3318-27.

20. Marchesan, S.; Da Ros, T.; Spalluto, G.; Balzarini, J.; Prato, M., *Bioorg Med Chem Lett* **2005,** *15* (15), 3615-8.

21. Yamakoshi, Y.; Umezawa, N.; Ryu, A.; Arakane, K.; Miyata, N.; Goda, Y.; Masumizu, T.; Nagano, T., *J. Am. Chem. Soc.* **2003,** *125* (42), 12803-12809.

22. Boutorine, A. S.; Tokuyama, H.; Takasugi, M.; Isobe, H.; Nakamura, E.; Helene, C., *Angew. Chem.* **1994,** *106* (23/24), 2526-9.

23. Tabata, Y.; Ikada, Y., *Pure Appl. Chem.* **1999,** *71* (11), 2047-2053.

24. Nakamura, E.; Isobe, H.; Tomita, N.; Sawamura, M.; Jinno, S.; Okayama, H., *Angew. Chem., Int. Ed.* **2000,** *39* (23), 4254-4257.

25. Roelofs, A. J.; Thompson, K.; Gordon, S.; Rogers, M. J., *Clin. Cancer Res.* **2006,** *12* (20, Pt. 2), 6222s-6230s.

26. Roux, C.; Dougados, M., *Drugs* **1999,** *58* (5), 823-830.

27. Coleman, R. E., *Cancer Treat. Rev.* **2001,** *27* (3), 165-176.

28. Delmas, P. D., *Lancet* **2002,** *359* (9322), 2018-2026.

29. Sambrook, P. N., *Curr. Pharm. Des.* **2002,** *8* (21), 1877-1883.

30. Hortobagyi, G. N.; Theriault, R. L.; Porter, L.; Blayney, D.; Lipton, A.; Sinoff, C.; Wheeler, H.; Simeone, J. F.; Seaman, J.; Knight, R. D.; Heffernan, M.; Reitsma, D. J., *N. Engl. J. Med.* **1996,** *335* (24), 1785-1791.

31. Theriault, R. L.; Lipton, A.; Hortobagyi, G. N.; Leff, R.; Gluck, S.; Stewart, J. F.; Costello, S.; Kennedy, I.; Simeone, J.; Seaman, J. J.; Knight, R. D.; Mellars, K.; Heffernan, M.; Reitsma, D. J., *J. Clin. Oncol.* **1999,** *17* (3), 846-854.

32. Rogers, M. J., *Curr. Pharm. Des.* **2003,** *9* (32), 2643-2658.

33. Jung, A.; Bisaz, S.; Fleisch, H., *Calcif Tissue Res* **1973,** *11* (4), 269-80.

34. Green, J. R.; Rogers, M. J., *Drug Dev. Res.* **2002,** *55* (4), 210-224.

35. Sietsema, W. K.; Ebetino, F. H.; Salvagno, A. M.; Bevan, J. A., *Drugs Exp. Clin. Res.* **1989,** *15* (9), 389-96.

36. Halasy-Nagy, J. M.; Rodan, G. A.; Reszka, A. A., *Bone (N. Y., NY, U. S.)* **2001,** *29* (6), 553-559.

37. Amin, D.; Cornell, S. A.; Gustafson, S. K.; Needle, S. J.; Ullrich, J. W.; Bilder, G. E.; Perrone, M. H., *J. Lipid Res.* **1992,** *33* (11), 1657-63.

38. Amin, D.; Cornell, S. A.; Perrone, M. H.; Bilder, G. E., *Arzneim.-Forsch.* **1996,** *46* (8), 759-762.

39. Strampel, W.; Emkey, R.; Civitelli, R., *Drug Saf.* **2007,** *30* (9), 755-763.

40. Lin, J.; Chen, I.-W.; Duggen, D. E., *Drug. Metab. and Dispos.* **1992,** *20* (4), 473-478.

41. Thompson, D. D.; Simmons, H. A.; Pirie, C. M.; Ke, H. Z., *Bone* **1995,** *17* (4 Suppl), 125S-133S.

42. McKenna, C. E.; Khawli, L. A.; Ahmad, *Phosphorus Sulfur Relat. Elem.* **1988,** *37*, 1-12.

43. Johnson, E. M.; Ambrose, C. G.; Hogan, H.; Cody, D., In *American Society for Bone and Mineral Research* Seattle, 2004.

44. Neale, J. R.; Richter, N. B.; Merten, K. E.; Taylor, K. G.; Singh, S.; Waite, L. C.; Emery, N. K.; Smith, N. B.; Cai, J.; Pierce, W. M., *Bioorganic & Medicinal Chemistry Letters* **2009,** *19* (3), 680-683.

45. Pierce, W. M., Jr.; Waite, L. C., *Proceedings of the Society for Experimental Biology and Medicine* **1987,** *186* (1), 96-102.

46. Shea, J. E.; Miller, S. C., *Advanced Drug Delivery Reviews* **2005,** *57* (7), 945-957.

47. Hirabayashi, H.; Fujisaki, J., *Clinical Pharmacokinetics* **2003,** *42* (15), 1319-1330.

48. Lin, J. H., *Bone* **1996,** *18* (2), 75-85.

49. Erez, R.; Ebner, S.; Attali, B.; Shabat, D., *Bioorganic & Medicinal Chemistry Letters* **2008,** *18* (2), 816-820.

50. Gittens, S. A.; Bansal, G.; Zernicke, R. F.; H., U., *Adv. Drug Deliv. Rev.* **2005,** *57* (7), 1011-1036.

51. Hengst, V.; Oussoren, C.; Kissel, T.; Storm, G., *International Journal of Pharmaceutics* **2007,** *331* (2), 224-227.

52. Hirabayashi, H.; Takahashi, T.; Fujisaki, J.; Masunaga, T.; Sato, S.; Hiroi, J.; Tokunaga, Y.; Kimura, S.; Hata, T., *Journal of Controlled Release* **2001,** *70* (1-2), 183-191.

53. Wang, D.; Miller, S.; Sima, M.; Kopeckova, P.; Kopecek, J., *Bioconjug. Chem.* **2003,** *14* (5), 853-859.

54. Elefteriou, F.; Ahn Jong, D.; Takeda, S.; Starbuck, M.; Yang, X.; Liu, X.; Kondo, H.; Richards William, G.; Bannon Tony, W.; Noda, M.; Clement, K.; Vaisse, C.; Karsenty, G., *Nature* **2005,** *434* (7032), 514-20.

55. Tierney, D. W., *J. Am. Optom. Assoc.* **1987,** *58* (9), 722-7.

56. Mehvar, R.; Brocks, D. R., *J. Pharm. Pharm. Sci.* **2001,** *4* (2), 185-200.

57. Bingel, C., *Chem. Ber.* **1993,** *126* (8), 1957-9.

58. Schwender, C. F.; Farber, S.; Blaum, C.; Shavel, J., Jr., *J. Med. Chem.* **1970,** *13* (4), 684-8.

59. Chiou, G. C. Y., *Biochem. Pharmacol.* **1981,** *30* (2), 103-6.

60. Kaplan, H. R., *Pharmacology of Antihypersensitive Drugs* **1980**, 317-23.

61. Leinweber, F. J.; Szpiech, J. M.; Di Carlo, F. J., *Pharmacology* **1978,** *16* (2), 70-7.

62. Jung, J. C.; Watkins, E. B.; Avery, M. A., *Synth. Commun.* **2002,** *32* (24), 3767-3777.